

1N-46

201483

51P

**NASA Technical Memorandum 104584**

**An Improved Gravity Model  
for Mars:  
*Goddard Mars Model-1 (GMM-1)***

**D. E. Smith, F. J. Lerch, R. S. Nerem,  
M. T. Zuber, G. B. Patel, S. K. Fricke,  
and F. G. Lemoine**

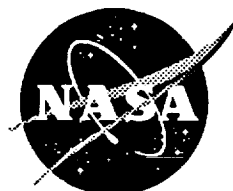
**May 1993**

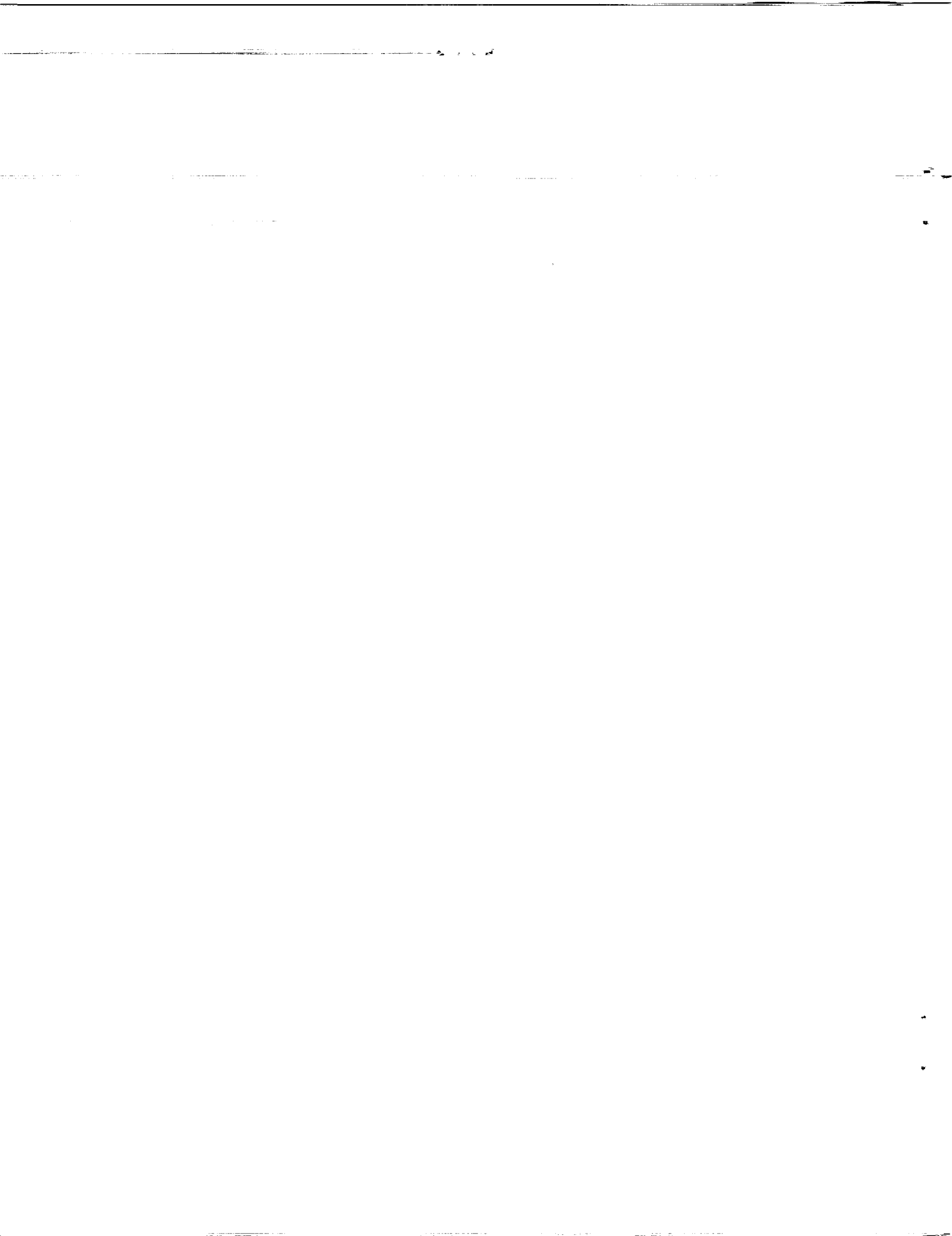
(NASA-TM-104584) AN IMPROVED  
GRAVITY MODEL FOR MARS: GODDARD  
MARS MODEL-1 (GMM-1) (NASA) 51 p

N94-23282

Unclas

G3/46 0201483





**NASA Technical Memorandum 104584**

RECEIVED  
GODDARD SPACE FLIGHT CENTER  
MAY 19 1993

RECEIVED  
GODDARD SPACE FLIGHT CENTER  
MAY 19 1993

**An Improved Gravity Model  
for Mars:  
*Goddard Mars Model-1 (GMM-1)***

**D. E. Smith, F. J. Lerch,  
R. S. Nerem, and M. T. Zuber**  
*Laboratory for Terrestrial Physics  
NASA Goddard Space Flight Center  
Greenbelt, Maryland*

**G. B. Patel**  
*Hughes-STX Corporation  
Lanham, Maryland*

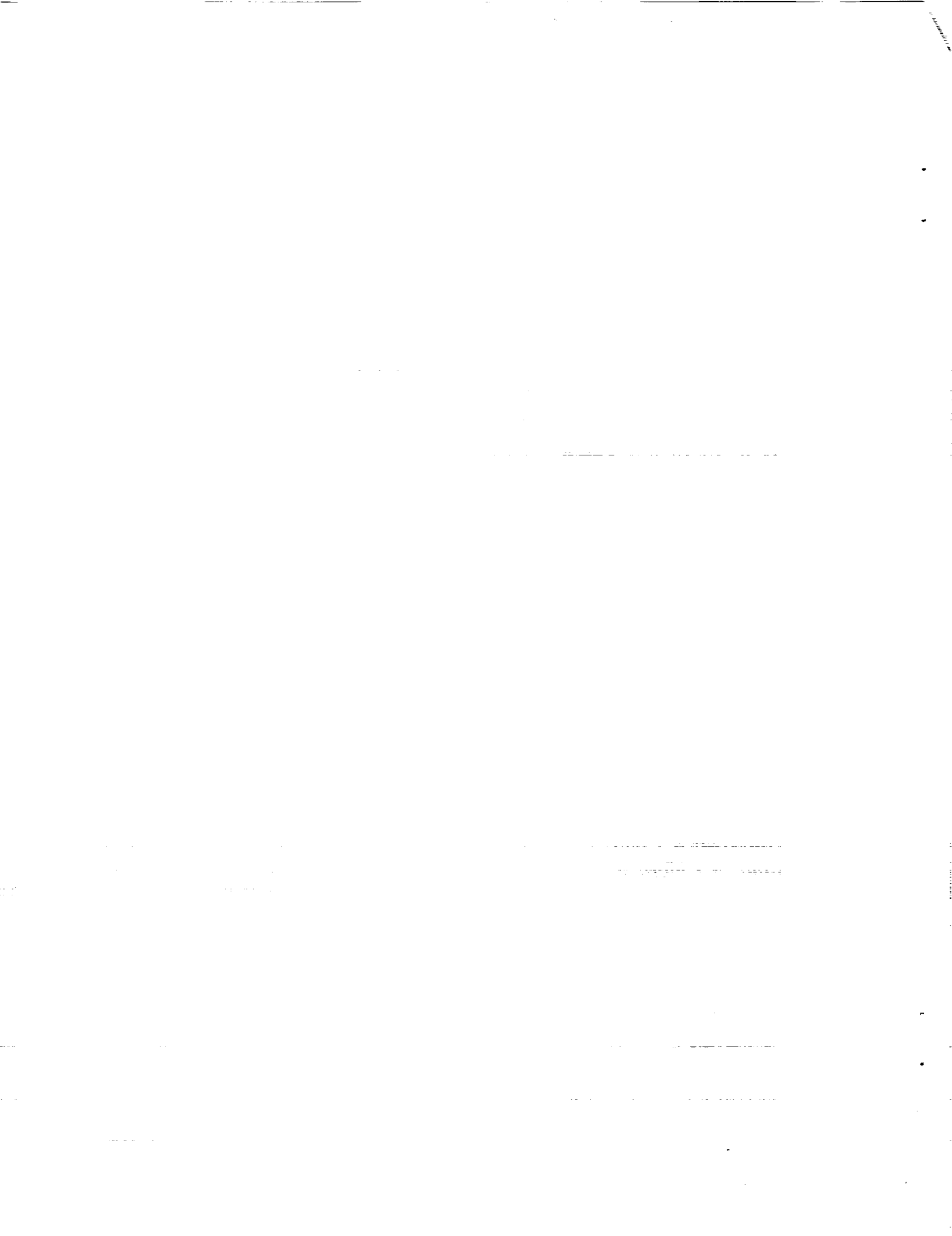
**S. K. Fricke**  
*RMS Technologies, Inc.  
Landover, Maryland*

**F. G. Lemoine**  
*Colorado Center for Astrodynamics Research  
University of Colorado  
Boulder, Colorado*



**National Aeronautics and  
Space Administration**

**Goddard Space Flight Center  
Greenbelt, Maryland 20771**

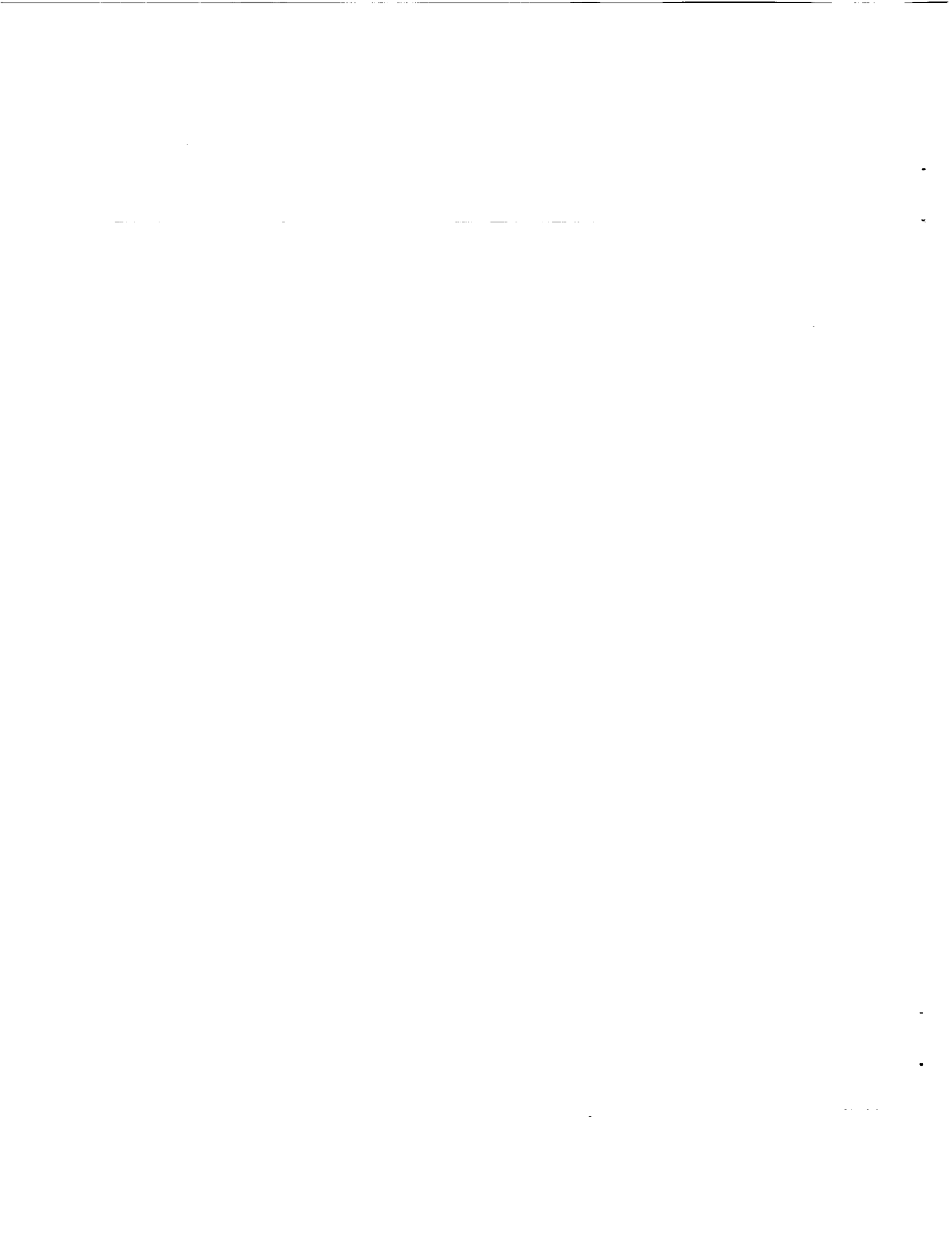


## ABSTRACT

Doppler tracking data of three orbiting spacecraft have been reanalyzed to develop a new gravitational field model for the planet Mars, GMM-1 (Goddard Mars Model-1). This model employs nearly all available data, consisting of approximately 1100 days of S-band tracking data collected by NASA's Deep Space Network from the Mariner 9, and Viking 1 and Viking 2 spacecraft, in seven different orbits, between 1971 and 1979. GMM-1 is complete to spherical harmonic degree and order 50, which corresponds to a half wavelength spatial resolution of 200-300 km where the data permit. GMM-1 represents satellite orbits with considerably better accuracy than previous Mars gravity models and shows greater resolution of identifiable geological structures. The notable improvement in GMM-1 over previous models is a consequence of several factors: improved computational capabilities, the use of optimum weighting and least squares collocation solution techniques which stabilized the behavior of the solution at high degree and order, and the use of longer satellite arcs than employed in previous solutions that were made possible by improved force and measurement models. The inclusion of X-band tracking data from the 379-km altitude, near-polar orbiting Mars Observer spacecraft should provide a significant improvement over GMM-1, particularly at high latitudes where current data poorly resolves the gravitational signature of the planet.

PRECEDING PAGE BLANK NOT FILMED

PAGE 11 INTENTIONALLY BLANK



## 1. INTRODUCTION

Knowledge of the gravitational field, in combination with surface topography, provides one of the principal means of inferring the internal structure of a planetary body. By removing the gravitational signal of the topography, the distribution of internal density anomalies associated with thermal or compositional differences can be estimated. Gravity can also be used to understand the mechanisms of compensation of surface topography, providing information on the mechanical properties and state of stress of the lithosphere.

The earliest global gravitational field models of Mars were derived from Doppler tracking data of the Mariner 9 spacecraft [Lorell *et al.*, 1972; 1973; Born, 1974; Jordan and Lorell, 1975; Reasenber *et al.*, 1975; Sjogren *et al.*, 1975]. These models provided estimates of low degree spherical harmonic gravity coefficients that yielded information on the oblateness and rotation vector orientation of Mars. Later models that incorporated data from Mariner 9 and the Viking 1 and 2 orbiters [Gapcynski *et al.*, 1977; Reasenber, 1977; Christensen and Balmino, 1979; Christensen and Williams, 1979] resolved higher degree gravity coefficients, showing the higher power in the Martian gravity field compared to Earth's, and the strong correlation of long wavelength gravity with topography. The subsequent inclusion of additional Doppler data by Balmino *et al.* [1982] resulted in what was then the highest resolution Martian gravitational model to date: an 18<sup>th</sup> degree and order field with half wavelength resolution of approximately 600 km. That field, which is characterized by a spatial resolution comparable to what was then the highest resolution (16x16) topographic model [Bills and Ferrari, 1978], was utilized in analyses of the state of stress of the Martian lithosphere and the isostatic compensation of surface topography [Sleep and Phillips, 1979, 1985; Banerdt *et al.*, 1982, 1992; Willemann and Turcotte, 1982; Esposito *et al.*, 1992]. However, the resolution and quality of the current gravity and topographic fields (particularly the latter) are such that the origin and evolution of even the most prominent physiographic features on Mars, namely the hemispheric dichotomy and Tharsis rise, are not well understood.

The resolution of the Balmino *et al.* [1982] gravity field was limited not by data density, but rather by the computational resources available at the time. Because this restriction is no longer a limitation, we have re-analyzed the Viking and Mariner data sets and have derived a new gravitational field, designated GMM-1 (Goddard Mars Model-1). The objectives of this study were: (1) to develop the best possible *a priori* gravitational field model for orbit determination of the Mars Observer spacecraft in support of the Radio Science and Mars Observer Laser Altimeter investigations, (2) to validate analysis techniques to be implemented in Mars Observer gravity modeling studies, and (3) to improve scientific interpretations of geophysical and geological data collected in previous missions to Mars.

GMM-1 is complete to spherical harmonic degree and order 50. The corresponding half wavelength resolution, which occurs where the coefficients attain 100% error, is 200-300 km where the data permit. In contrast to previous models, GMM-1 was solved to as high degree and order as necessary to nearly exhaust the attenuated gravitational signal contained in the tracking data. This was possible mainly due to the use of

optimum weighting and least squares collocation solution techniques [Lerch *et al.*, 1979], which stabilized the behavior of the solution at high degree and order where correlation and data sensitivities become problematic. As discussed later, the extension of the model to high degree and order significantly reduced errors resulting from spectral leakage coming from the omitted portion of the gravitational field beyond the limits of the recovered model. GMM-1 has a higher spatial resolution than preliminary versions of this model [Smith *et al.*, 1990a; Zuber *et al.*, 1991], and in addition is fully calibrated to give a realistic error estimate from the solution covariance.

In the following sections we discuss the development of GMM-1 and make a detailed comparison of the field with the previous model of Balmino *et al.* [1982]. We also include an error analysis and a discussion of the implications of GMM-1 for Martian geophysics and for navigation and precision orbit determination in support of the upcoming Mars Observer Mission.

### 1.1 General Approach of Gravitational Field Recovery

Figure 1 shows a flow chart of the procedure used in the recovery of the gravitational field model. The data were processed using the GEODYN/SOLVE orbit determination/estimation programs [Putney, 1977]. These programs have previously been used in the derivation of a series of Goddard Earth gravitational Models, GEM, [e.g. Lerch *et al.*, 1979; Marsh *et al.*, 1988; 1990], and have been adapted for the analysis of planetary tracking data [Smith *et al.*, 1990b; Nerem *et al.*, 1993]. GEODYN provides orbit determination and geodetic parameter estimation capabilities, and numerically integrates the spacecraft Cartesian state and the force model partial derivatives employing a high-order Cowell predictor-corrector method. The force modeling includes a spherical harmonic representation of the gravity field, as well as a point mass representation for the Sun, Earth, Moon, and the other planets. Atmospheric drag, solar radiation pressure, measurement and timing biases, and tracking station coordinates can also be estimated. The least squares normal equations formed within GEODYN may be output to a file for inclusion in error analyses and parameter estimations. The SOLVE program then selectively combines the normal equations formed by GEODYN to generate solutions for the gravity field and other model parameters. The resulting gravitational model may be input back into GEODYN for residual analyses.

### 1.2 Representation of The Gravitational Potential

The gravitational potential at spacecraft altitude,  $V_M$ , is represented in spherical harmonic form as

$$V_M = \frac{GM}{r} + \frac{GM}{r} \sum_{l=2}^N \sum_{m=0}^l \left( \frac{r_M}{r} \right)^l \bar{P}_{lm}(\sin\phi) [\bar{C}_{lm} \cos m\lambda + \bar{S}_{lm} \sin m\lambda] \quad (1.1)$$



where  $r$  is the radial distance from the center of mass of Mars to the spacecraft,  $\phi$  and  $\lambda$  are the areocentric latitude and longitude of the spacecraft,  $r_M$  is the mean radius of the reference ellipsoid of Mars,  $GM$  is the product of the universal constant of gravitation and the mass of Mars,  $P_{lm}$  are the normalized associated Legendre functions of degree  $l$  and order  $m$ ,  $C_{lm}$  and  $S_{lm}$  are the normalized spherical harmonic coefficients which were estimated from the tracking observations to determine the gravitational model, and  $N$  is the maximum degree representing the size (or resolution) of the field. The gravitational force due to Mars which acts on the spacecraft corresponds to the gradient of the potential,  $V_M$ .

## 2. REFERENCE SYSTEMS FOR DSN TRACKING OF MARS SPACECRAFT

Spacecraft orbiting Mars are tracked from Earth through the NASA DSN (Deep Space Network) tracking stations at Goldstone (California), Canberra (Australia) and Madrid (Spain). The adopted planetary ephemeris for Earth, Mars, and the other planets was the JPL DE-96 system [Standish *et al.*, 1976].

The inertial coordinate system for the Earth is defined by the direction of the Earth's rotation axis and the location of the vernal equinox. The orientation of the Mars rotation axis is specified by the right ascension and declination of the Martian pole, as given in Davies *et al.* [1986; 1992]. The z-axis of the Mars inertial coordinate system is the instantaneous Mars rotation axis. The direction of the x-axis (the IAU vector) is defined to be the intersection of the instantaneous Mars equator with the mean Earth equator of the appropriate ephemeris epoch. For this analysis, 1950.0 was chosen as the epoch, and thus the IAU vector was defined with reference to the Earth Mean Equator and Equinox of 1950.0 (EME50). The prime meridian of Mars is defined in Davies *et al.* [1989]. At the beginning of this analysis, tests were performed using a reference date and planetary ephemeris of 2000.0 but results showed that the 1971 Mariner 9 data and 1976-78 Viking data were better satisfied with a reference date of 1950.0.

Various reference system constants that were used are given in Table 1.

## 3. DATA SUMMARY AND ORBITAL SENSITIVITY OF GRAVITY

### 3.1 Satellite Orbital Characteristics

The Mariner 9 (M9), Viking Orbiter 1 (VO1) and Viking Orbiter 2 (VO2) spacecraft were in highly eccentric orbits with periods of approximately one day for Viking 1 and 2 and one-half day for Mariner 9. The satellite orbit characteristics are summarized in Table 2. The orbital periods are nearly commensurate with the rotational period of Mars (24.623 hr) which produce dominant resonant perturbations [Kaula, 1966] for all orders  $m$  of the Viking spacecraft (24 hour period) and for the even orders of M9 (12 hour period). The resonant periods range mostly from about 1 to 50 days for shallow resonant terms and also include deep (very long)

resonant periods. The beat period, or fundamental resonant period, identifies the shift (or "walk") in successive ground tracks and is useful in mapping the orbital coverage over Mars (a plus sign represents an eastward "walk" and a negative sign for a westward "walk"). The beat period changes after each maneuver of the Viking 1 and 2 spacecraft [Snyder, 1979]. For example, an orbit maneuver by VO2 on March 2, 1977 produced a very slow walk to synchronize with the Viking Lander (VL2). Subsequently on April 18, 1977, another maneuver resulted in a walk around the planet in 13 revolutions, producing a beat period of 12 days. Strong resonant perturbations of long period were produced on VO1 commencing on Dec. 2, 1978 to provide a slow walk around the planet. Mission events such as leakages, attitude control jetting, and other phenomena that cause variations in the orbital periods are described by Snyder [1977; 1979].

The 300-km periapsis altitude orbits of VO1 and VO2 provide the strongest contribution of data to the solution for the higher degree terms, particularly the VO1 low orbit with a range of  $180^\circ$  for the argument of periapsis ( $\omega$ ) as compared to  $25^\circ$  for the VO2 low orbit. The observing period for the VO1 low orbit shown in Table 2 covers almost 2 years from 77-03-12 to 79-01-27, and the periapsis point varies in latitude from  $+39^\circ$  to  $-39^\circ$  during this period. The VO1 low orbit provides about a  $9^\circ$  ground track "walk" per revolution for the 1 1/2 year period from 77-07-01 to 78-12-02. This corresponds to a "near repeat" of the ground track for a 39-day period. After the 39 day near repeat period the orbital ground track shifts by  $1.8^\circ$  from the previous repeat track which corresponds to a deep orbital resonance with a period of about 200 days. This produces, over a 200-day coverage, a global grid ( $39^\circ$  latitude) with approximately  $1.8^\circ$  ground track separations and provides for a high resolution recovery of the gravity field.

## 3.2 S-band Doppler Tracking Data Used in the Solution

### 3.2.1 Data Summary

The data set consisted of 265 orbital arcs representing over 1100 days of S-band Doppler tracking data from the Mariner 9 and Viking 1 and 2 spacecraft, collected by the Deep Space Network between 1971-1978. These data, grouped by satellite periapsis altitude and inclination, are summarized in Table 3. In total over 230,000 total observations were included in the GMM-1 solution.

### 3.2.2 Data Characteristics

The data consist of two-way S-band (2.2 GHz) Doppler measurements compressed to 60 seconds (1 minute data points). Data far removed from periapsis (approximately greater than 12,000 km altitude) were compressed over 10 minute intervals.

All observations were collected by three DSN sites located at Goldstone, Madrid, and Canberra. They were processed in the differenced-range Doppler formulation taking into account relativistic bending due to the

Sun [Moyer, 1971]. Observations near satellite periapsis are most valuable for determining the gravity field and periapsis is generally observable by at least one of the DSN sites except when occulted by Mars. The data distribution and coverage per satellite orbit is discussed in Section 3.4.

The signal is significantly degraded in precision during solar conjunction due to the solar plasma effects when its path comes within  $5^\circ$  of the Sun from Mars. This occurred for a period of about 1 month beginning November 7, 1976 for seven Viking 1 and 2 arcs. The data were downweighted in the solution for this period.

### 3.3 Spectral Sensitivity of Gravity Signal

The spectral sensitivity of the gravity field is analyzed for the Mariner 9, VO1 and VO2 orbits. Sensitivity for the high degree terms ( $>30$ ) is the main area of interest and these are compared with a threshold level corresponding to the precision of the DSN signal. The signal when compressed to 1 minute data points has a precision of  $1 \text{ mm s}^{-1}$  and approximately  $0.3 \text{ mm s}^{-1}$  for 10 minute data points. A sensitivity study for the above Mars orbiters has been made by *Rosborough and Lemoine* [1991] and *Lemoine* [1992] for terms through degree 20. Analysis for the high degree terms is discussed in detail in *Lerch et al.* [1993]. A brief summary is given here.

The orbit perturbations were studied using linear perturbation theory, and through numerical integration by GEODYN. The gravity signal for sensitivity analysis employed a form of Kaula's rule,  $13 \times 10^{-5} / l^2$ , for terms of degree  $l$ , which was obtained by *Balmino et al.* [1982] for the power spectrum of Mars. The velocity perturbations were compared with the noise of the DSN Doppler data. Both the analytical and numerical studies confirm the importance of the resonance perturbations in determining the satellite sensitivity to the Mars gravity field.

The resonances on the Viking spacecraft fall into three classes: (1) resonances at the low orders (characterized by periods of up to 40 days), (2) long period resonances (periods greater than 50 days) at specific higher orders, and (3) intermediate resonances at the other orders. The long period resonances result from a near repeat of the ground trace after an integer number of spacecraft revolutions. Thus, referring to Table 2, the Viking 1 orbit from July 1, 1977 through December 2, 1978, the near repeat of the ground trace (to within  $1.8^\circ$ ) after 38 revolutions produces a perturbation at order 38 with a period of about 200 days.

The analytical velocity spectrum by degree is presented in Table 4 for both M9 and the 300-km, 800-km, and 1500-km VO1 and VO2 orbits. The analytical velocity spectrum is obtained by computing the Kepler element perturbations using *Kaula's* [1966] theory, and then mapping these to velocity space. Since we are interested in the satellite sensitivity to the gravity field over the periods of the arc lengths of data used in the GMM-1 solution, perturbations with periods greater than 40 days were excluded. In addition, those perturbations with periods between eight and 40 days have been prorated to eight days by the factor  $8/\text{period}$ . The VO1 300-km orbit has a sensitivity in excess of  $1 \text{ mm s}^{-1}$  (the accuracy of the S-band data) out to degree 50. In contrast,

the VO2 300-km orbit is sensitive only to terms out to approximately degree 30. As the periapsis altitude is raised, the sensitivity in degree is diminished. The limit is degree 18 for the VO2 800-km orbit, and degree 11 for the VO1 1500-km orbit. The M9 orbit has stronger perturbations than the VO1 1500-km orbit by virtue of its closer average distance to Mars, with its twice per day revolution, and smaller orbital eccentricity.

The sensitivity was also evaluated through numerical integration using the GEODYN program for the VO1 300-km orbit. The spectral rms velocity perturbation by order is shown in Figure 2 for different arc lengths. The results show sensitivity greater than  $1 \text{ mm s}^{-1}$  for the high degree and order terms for arc lengths greater than three days. For arcs of three days, the limit in sensitivity is approximately order 30, whereas for the one day arcs the limit in sensitivity is approximately order 20. The increase in sensitivity results from the sampling of the medium period resonance perturbations. Although these results suggest it would be beneficial to process the VO1 300-km data in batches of 8 to 16 days, this was not possible because of insufficient tracking coverage and errors in the nonconservative force models.

For the highly eccentric Viking orbits, the sensitivity of spherical harmonic coefficients depends not only on the periapsis altitude, but also on the location of the argument of periapsis. The GEODYN spectrum of rms velocity perturbations sampled by degree and order are given for an eight day arc for two VO1 300-km orbits in 1978. In the first arc, beginning January 15, 1978, periapsis is located near the equator ( $\omega \sim 175^\circ$ ). In the second test arc, beginning December 20, 1978, the periapsis is located near  $39^\circ\text{S}$  ( $\omega \sim 269^\circ$ ). When  $\omega$  is near  $180^\circ$ , the orbit tends to be sensitive to terms of high degree and high order, whereas when  $\omega$  is near  $270^\circ$ , the orbit is sensitive to terms of high degree and low order (see Figure 3).

Another important characteristic of these eccentric orbits is that significant sensitivity to the high degree terms exists over a broad range of altitudes. As a demonstration, for the VO1 arc described in Figures 2 and 3 (epoch 01-15-78), the perturbations for terms of order 25 (degrees 31 to 50) are shown over a revolution in Figure 4. For these terms, significant sensitivity is apparent up to an altitude of 10,000 km, covering half of an orbit revolution.

In summary, the high degree sensitivity of the Viking Orbiter tracking data to the gravity field of Mars is determined by the periapsis altitude, location of the argument of periapsis, and the length of the arcs used to process the tracking data.

### 3.4 Distribution of Observational Coverage

The groundtrack for each of the Doppler observations is plotted in Figures 5a and 5b for a complete set of ground tracks covering all major data sets used in the solution. The separation between ground tracks for the orbital data sets is indicated in the figures by the term "walk". Also the data span is given along with the "walk" to depict the extent of the coverage over all data of this type as originally given in Table 2. In these figures we can see the extent of periapsis coverage of the VO1 low orbit ( $39^\circ$  latitude) which is well complemented in the northern hemisphere by the VO2 low orbit. These figures show reasonably good global data coverage for the

VO1 low orbit, VO2 low orbit, VO2 800 km orbit, and also for M9. The global coverage provides for good separability of the lower degree terms of the gravity field and possibly out through degree 30 considering the strong sensitivities to these terms. Figure 6 shows the combined coverage of the low orbits of VO1 and VO2 from observations with altitudes less than 5000 km and it shows coverage by different levels of altitude over 300-km. This low altitude data coverage of the observation points along the ground tracks for the VO1 low orbit is seen to be complemented by the VO2 low orbit, particularly in the Northern Hemisphere. However, the lack of complete data coverage near periapsis indicates that separability will not be complete for the high degree terms (30 to 50) as noted above in the argument of periapsis coverage for VO2.

Nevertheless, the result from Figure 6 indicates that there is great sensitivity to the higher degree terms for altitudes less than 2000 km for the low altitude Viking orbits. Hence we may expect that the ground track coverage for the combined VO1 and VO2 low orbits, particularly for the observed coverage with altitude less than 500 km over a wide area, will provide for good resolution of localized geophysical features in the vicinity of these ground tracks.

## 4. MODELING

### 4.1 Physical Model

Because the Viking and Mariner data do not provide uniform spatial coverage of Mars, the application of *a priori* constraints was critical to the development of a high degree and order solution. The Viking and Mariner data were initially processed using the gravity model of *Balmino et al.* [1982]. However, in the final iteration to produce GMM-1, an intermediate solution, MGM-635, was used as the *a priori* model.

The gravitational effects of the Martian solid body tide were included in the satellite force model, and a value of  $k_2 = -0.05$  was adopted [*Christensen and Balmino, 1979*]. The effects of atmospheric drag were incorporated into the satellite force model using a spherical model for the satellite body and the atmospheric density model developed by *Culp and Stewart* [1984]. The coefficient of drag,  $C_D$ , was adjusted once per data arc, except for the VO1 and VO2 low periapsis orbital arcs, where  $C_D$  was adjusted once per day. Solar radiation forces were calculated using a spherical model for the spacecraft body, and adjusting a reflectivity coefficient,  $C_R$ , once per data arc.

The solar flux at Mars at a given time was scaled from the Earth value for that date to the actual distance of the spacecraft from the Sun. One range rate bias was estimated for each tracking station per arc. The measurements were corrected for tropospheric effects using the Hopfield model [*Hopfield, 1971*]. The tracking data records did not contain meteorological data or tropospheric corrections, thus the corrections were computed assuming standard temperature, humidity, and pressure, scaled to reflect the station height above sea level.

Third body gravitational perturbations on the spacecraft were computed from the point mass gravitational forces due to the Sun, the Earth-Moon system, the other planets, and Phobos, one of Mars' natural satellites. In addition, Geodyn was modified to read an ephemeris for Phobos and to add the point mass gravitational acceleration due to Phobos to the total spacecraft acceleration. The ephemeris of Phobos was prepared at GSFC by processing optical measurements obtained from the Mariner 9 and Viking Orbiter images of Phobos [Duxbury and Callahan, 1988; 1989].

## 4.2 Method of Solution

### 4.2.1 Least Squares with A Priori Constraints

The method of solution is a modified least squares process [Lerch *et al.*, 1979; Schwartz, 1976; 1978] which minimizes the sum ( $Q$ ) of signal and noise as follows

$$Q = \sum_{l,m} \frac{\bar{C}_{lm}^2 + \bar{S}_{lm}^2}{\sigma_l^2} + \sum_i \sum_{obs,} \frac{r_{ik}^2}{\sigma_k^2} f_k \quad (4.1)$$

where the signal is given by  $\bar{C}_{lm}$ ,  $\bar{S}_{lm}$  which are the normalized spherical harmonics comprising the solution coefficients. The parameter  $\sigma_l = 13 \times 10^{-5} / l^2$  is the rms of the coefficients of degree  $l$  (*a priori* power rule) and is introduced to permit solutions to degree and order 50. This expression, which is based upon Kaula's rule [Kaula, 1966], has been obtained by Balmino *et al.* [1982] and represents the power in that gravity model. The noise given by  $r_{ik}$  is the observation residual (observed-computed) for the  $i^{\text{th}}$  observation of satellite tracking data set type  $k$ ,  $\sigma_k$  is the rms of observation residuals of data type  $k$  (generally significantly greater than the *a priori* data precision), and  $f_k$  is a downweighting factor to compensate for unmodeled error effects for each data type  $k$  (ideally  $f_k=1$  for pure noise).

The optimum weighting method estimates the combined weights directly, namely

$$w_k = \frac{f_k}{\sigma_k^2} \quad (4.2)$$

When minimizing  $Q$  above using the least squares method, the normal matrix equation and error covariance is obtained as follows:

$$N \hat{x} = R \quad (4.3)$$

where  $\hat{x}$  is the solution,  $N$  is the normal matrix,  $R$  is the vector of residuals, and

$$V = N^{-1}, \quad N = \sum w_k N_k \quad (4.4)$$

is the approximate form for the variance-covariance error matrix which must be calibrated by adjusting the weights.  $N_k$  is the contribution for each satellite data set  $k$  to the normals, where  $k = 0$  corresponds to the normal equations for the satellite *a priori* coefficient constraints for which  $N_0$  is the matrix of Kaula constraints and the weight  $w_0$  is fixed at unity for the constraints.

The process of minimizing both signal (by application of the Kaula power rule constraints) plus noise in (4.1) is also known as collocation [Moritz, 1978]. The constraints bias the coefficients towards zero where they are poorly observed. With the conventional least squares approach (noise-only minimization) there is a problem of separability due to the strong correlation between many of the high degree coefficients. The absence of collocation ( $w_0 = 0$  in (4.4) for GMM-1) results in excessively large power in the adjustment of the potential coefficients as in Figure 7. Hence, we see the benefit of the constraints which permit resolution of the high degree terms wherever the data permits and provide control of aliasing in the solution.

#### 4.2.2 Data Weighting and Error Calibration

The weighting technique and error calibration [Lerch *et al.*, 1988; Lerch, 1991] of the solution (equations 4.1-4.4) is based upon subset solutions. The subset solution ( $C_k$ ) is formed by deleting a major data set  $k$  from the complete solution ( $C$ ). The weight  $w_k$  is adjusted as in equation (4.7) below by requiring that

$$\|\Delta C_k\| = K_k \sigma (\Delta C_k) \quad (4.5)$$

where  $K_k$  is an error calibration factor which ideally should equal to unity,

$$\begin{aligned} \|\Delta C_k\| &= \left\{ \sum (C - C_k)^2 \right\}^{\frac{1}{2}} \\ \sigma (\Delta C_k) &= \left\{ \sum (\sigma^2 - \sigma_k^2) \right\}^{\frac{1}{2}} \end{aligned} \quad (4.6)$$

and where  $\sigma_k^2$  and  $\sigma^2$  are respectively the variance of the subset and the complete solutions. The sum in (4.6) is over all the coefficients, and the scale factor  $K_k$  is needed for the errors since the error covariance in (4.4) is only an approximation [Lerch, 1991].

The new weights,  $w_k'$ , should be adjusted so that each  $K_k$  converges to 1 for all  $k$ , and the new weights are computed from

$$w_k' = \frac{w_k}{K_k^2} \quad (4.7)$$

The process is iterated by forming a new complete solution and subset solutions from the new weights, and this process may continue until the weights converge.

In a case where two solutions are based upon independent data, then (in the above notation) for a single coefficient parameter the two estimates give

$$E(C - \bar{C})^2 = \bar{\sigma}^2 + \sigma^2 \quad (4.8)$$

whereas in Table 4.1 the data for the subset solution is wholly embedded in the complete solution in which case

$$E(C - \bar{C})^2 = \bar{\sigma}^2 - \sigma^2 \quad (4.9)$$

as indicated by (4.6). This means that in our case the covariance between the square of the difference of the two estimates of the coefficients is equal to the difference of the variances of the subset and complete solutions.

Thus, (4.8) and (4.9) represent extremes in estimation, complete independence and complete dependence.

## 5. RESULTS OF THE GMM-1 SOLUTION

### 5.1 Description of Solution

GMM-1 is a 50 x 50 spherical harmonic gravity model. There are a total of 5250 estimated parameters: 2597 gravity coefficients plus  $GM$ , and the arc parameters. The GMM-1 gravity coefficients through degree and order 50 are shown in Appendix A. Calibrated accuracy estimates of the coefficients have also been obtained for the model.

### 5.2 Gravity Model Tests Using Orbital Observation Residuals

Orbital arcs have been selected from the 7 major data sets summarized in Table 3 and used to test the orbital accuracy of the model by fitting the DSN Doppler data. Observation residuals have been computed from our 50x50 model and compared with the prior best available 18x18 gravity model of *Balmino et al.* [1982]. Table 5 is a compilation of orbit tests for 14 arcs. Each arc is fit using the *Balmino et al.* field and GMM-1. For all 14 test arcs, the RMS residual fits are significantly smaller, sometimes 5 to 10 times smaller, when computed using GMM-1 than when using the *Balmino et al.* field. Table 6 summarizes the results of orbit prediction tests for a subset of the arcs in Table 5. The orbits obtained in the orbit accuracy tests are projected forward in time 2 or 3 days. Then RMS residual fits are compared for the data in the predicted time periods. Again, the fits are



significantly smaller when computed using GMM-1 than when using the *Balmino et al.* field. The improvements in the fits is not entirely due to the increased resolution of GMM-1. An 18x18 version of GMM-1 outperformed the 18x18 model of *Balmino et al.* in all cases except the 300-km VO1 and VO2 orbits, for which the performance was comparable.

### 5.3 Analysis of the Gravity Coefficients

Figure 8 is a plot of the degree variance of the coefficients (power) and error variance of GMM-1 per degree. Also plotted are the power of the 18x18 gravity field [*Balmino et al.*, 1982] and a power rule ( $13 \times 10^{-5} / l^2$ ) taken from *Balmino et al.* [1982], which is the basis of the constraint matrix used in GMM-1. The plot shows that for degrees less than 15, the power spectrum of GMM-1 and the *Balmino et al.* field are about the same. However, above degree 15, GMM-1 drops below while the *Balmino et al.* field rises above the power spectrum of Balmino's rule. The upward turn of the *Balmino et al.* field is undoubtedly due to aliasing. Aliasing adversely affects the performance of a gravity field with respect to orbit fits from independent data, orbit predictions, and other geophysical information which are derived from the gravity coefficients. The truncation level of GMM-1 at degree 50 is high enough so that the high degree gravity signal is not significantly aliased into the lower degree terms.

The power spectrum of GMM-1 drops below the values of the power rule for high degrees. Above degree 22, the errors of the coefficients are larger than the coefficients themselves. This drop off in the power spectrum occurs because the drag parameters (once per day values) are absorbing part of the gravity signal. Also, the high degree terms are highly correlated and hence the effect of the power rule constraint in the solution is quite strong which further explains the small power for these terms. However, because the *a priori* constraint does not have a major effect on the solution, the terms do contain information on the short wavelength gravity field in the vicinity of the spacecraft periapses. While the power in the field falls below that predicted by the power rule at high degrees, the field is a better representation of the true gravitational signature of the planet at those wavelengths than would be the case if the field were solved to lower degree and order and all of the high degree and order coefficients were constrained to zero.

Figure 9 shows the coefficient differences between GMM-1 and the 18x18 gravity field. While the rms differences per degree are about the size of Balmino's rule for terms above degree 10, the differences between particular ( $\dot{C}_{lm}, \dot{S}_{lm}$ ) pairs even for lower degree terms are seen to be quite large. In fact, the rms differences for lower degree terms are over an order of magnitude greater than the error estimates of GMM-1 as given in Figure 8. The coefficient discrepancy between these models reflects the large differences seen in the orbital residuals for the two models as shown in Table 5.

### 5.4 Calibration of Gravity Model Errors

The calibration of the gravity model error estimates is based upon the method described in Section 4.2.2 and is developed in greater detail by *Lerch et al.* [1991]. In the application of this method, weights of basic observation sets from different orbits are adjusted based on subset solutions. The data is separated into 7 groups (see Table 6) yielding 7 subset solutions for the weight adjustment. In Table 6 each group is assigned an *a priori* data weight which is based on our experience in computing previous gravity solutions. For example, the Viking 1 1500-km data group is assigned an error of  $1 \text{ cm s}^{-1}$  while Viking 1 300-km data group is assigned an error of  $.71 \text{ cm s}^{-1}$  [wt.= $1/((.71)^2-2)$ ]. The larger errors (indicating down-weighting) for the data sets of Viking 1 at 1500-km and Viking 2 at 1500-km ( $55^\circ$  inclination) are due to the synchronous (repetitive) nature of the orbits (over the Viking Landers) as shown in Table 2 and in Figure 5a and 5b for the data distribution. The calibration factors (*k*) given in Table 7 indicate that the model is reasonably well calibrated where a factor of  $k=1$  indicates perfect calibration.

### 5.5 Error Analysis

The error covariance matrix, which is calibrated in Section 5.4, was used to project the orbital errors in satellite position and velocity. Table 8 shows the projected errors for M9, V01-300 km, VO@-300 km, and MO for a 6-day arc length. The results for the Mars Observer orbit are of special interest since these errors will affect the orbit determination. Figures 10 and 11 give respectively the error spectrum by degree and order for the radial and along-track position components of Mars Observer (cross-track errors are similar to the radial errors). Note the largest error is shown for resonant order 25 indicating that a field complete to at least degree 30 is required to reasonably model these coefficients based upon the error spectrum by degree.

### 5.6 Recovery of GM

In the GMM-1 solution, the *GM* of Mars was adjusted along with the other coefficients of the Mars gravity field. The value of *GM* determined in the solution was  $42828.36 \pm 0.05 \text{ km}^3 \text{ s}^{-2}$ . *Lemoine* [1992] analyzed a smaller set of Viking and Mariner 9 Doppler data as well as Viking Orbiter range data and determined a value of *GM* of  $42828.40 \pm 0.03 \text{ km}^3 \text{ s}^{-2}$ . The estimates of the Mars *GM* from Mariners 4, 6 and 9 [Null, 1969; Anderson et al., 1970; O'Neill et al., 1973] are in close agreement with the GMM-1 value. The Mariner 4, 6 and 9 values are especially interesting since they are derived from tracking of spacecraft from a flyby of the planet Mars. In these cases, the estimate of the Mars *GM* is largely uncoupled from the remaining coefficients of the Mars gravity field.

## 6. GEOPHYSICAL IMPLICATIONS

Figure 12 shows free air gravity anomalies computed from GMM-1 complete to degree and order 50, and Figure 13 displays accompanying gravity anomaly errors computed from the error covariance matrix. As

illustrated in Figures 5 and 6, the satellites used in this study are characterized by a complicated distribution of low altitude data. The shortest wavelengths resolved (200-300-km half wavelength) occur within the latitudinal band of 40° corresponding to the data coverage from the VO1 low orbit. This region also includes the periapsis coverage (0° to 30° latitude) of the VO2 low orbit as seen in Figure 6. That figure also shows that above 40° N latitude there is still strong coverage of periapsis extending to 63°N latitude particularly for the VO2 800-km altitude orbit. This coverage is reflected in the gravity anomaly error map which shows more longitudinal structure and better resolution than in the corresponding southern hemisphere beyond the region of 40°S latitude.

In Figure 12, the free air anomalies are overlain by contours of topography. The topographic field is a spherical harmonic expansion, also complete to degree and order 50, of the Mars Digital Elevation Model [DEM; *Wu et al.*, 1986]. The spherical harmonic topographic model was defined to have zero mean elevation, and so while the spherical harmonic and DEM have similar hypsometric distributions, elevation values from the former are offset by approximately two km from the latter.

As in previous studies, the gravity anomalies correlate well with principal features of Martian topography, including volcanic shields, impact basins and the Valles Marineris. Most major features exhibit anomalies with considerably higher magnitudes than in previous models. GMM-1 also exhibits gravity anomalies in association with some observed structures that were not previously detected. For example, GMM-1 resolves all three Tharsis Montes, while the model of *Balmino et al.* [1982] fails to resolve the central volcano in the line, Pavonis Mons. GMM-1 also shows considerably more detail associated with the Valles Marineris, and for several of the major impact basins including Isidis and Argyre. However, it is important to interpret short wavelength features resolved in the model with caution, as the coefficients associated with the highest degree and order terms are 100% in error.

One of the most prominent physiographic features on Mars is the hemispheric dichotomy, which is characterized by a 2-km elevation difference between the northern and southern hemispheres of Mars. However, the dichotomy does not have a distinct gravitational signature associated with it. This indicates that the dichotomy boundary is isostatically compensated at the resolvable wavelengths of GMM-1, perhaps due to a change in crustal thickness across the boundary, as suggested in previous studies [*Phillips and Saunders*, 1975; *Lambeck*, 1979; *Phillips and Lambeck*, 1980; *Phillips*, 1988].

It is significant to note that several prominent anomalies in GMM-1 fail to correlate with observed surface features. These include a 300-mgal negative anomaly on the western edge of Tharsis (lon=200°E, lat=+20°N) and a 200-mgal positive anomaly in Utopia (lon=105°E, lat=50°N). Both of these areas are in the northern hemisphere and may have been resurfaced. These features were also present in the field of *Balmino et al.* [1982], but the anomalies were smaller in magnitude.

As for the gravity anomaly representation of the field, the geoid from GMM-1 as shown in Figure 14 exhibits a higher dynamic range of power (2300 m vs. 1950 m) than the model of *Balmino et al.* [1982]. The distribution of geoid errors shows a similar pattern to the gravity anomaly errors.

A detailed geophysical interpretation of GMM-1, which includes a spectral analysis of the gravity and topography fields and a global inversion of the fields for simultaneous estimations of density anomalies in the Martian crust and mantle, is presented in a companion paper by *Bills et al.* [manuscript in preparation, 1993].

## 7. SUMMARY

Re-analysis of Doppler tracking data from the Mariner 9 and Viking 1 and 2 spacecraft has led to the derivation of a 50<sup>th</sup> degree and order gravitational model for Mars. The model has a maximum (half wavelength) spatial resolution of 300-km where the data permit, which represents a factor of two improvement over that attained by the previous field of *Balmino et al.* [1982] which utilized essentially the same data. Probable reasons for the significant improvement achieved include: increased computational capabilities, the application of collocation and optimum data weighting techniques in the least squares inversion for the field, and the use of longer arcs (days vs. hours) than used previously for Viking low altitude data made possible by improved force and measurement models.

Error analyses based on the observation data, derived power spectrum, and comparison with topography demonstrate that this field represents the orbits with considerably better accuracy and shows greater resolution of identifiable geological structures than previous models. The model also shows a greater dynamic range of power in both the gravity anomaly field and the geoid. The inclusion of X-band tracking data from the 379-km altitude, near-circular, polar orbit of Mars Observer will allow significant improvement of the Martian gravitational field [*Smith et al.*, 1990b; *Esposito et al.*, 1990; *Tyler et al.*, 1992], with the greatest refinement occurring at high latitudes far removed from the Mariner 9 and Viking 1 and 2 periapsis latitudes. That gravitational field, in combination with topography data from the Mars Observer Laser Altimeter (MOLA) [*Zuber et al.*, 1992] will allow detailed analyses of Mars' internal structure, state of lithospheric stress, and mechanisms of isostatic compensation of surface topography.

**Acknowledgements:** We are grateful to George Balmino for providing the DSN tracking data used in the solution and for suggestions and analysis associated with the development of our solution including comparisons of gravity models with his JEEP software. We also thank Bill Sjogren, Pat Esposito, and Ed Christensen for suggestions concerning the development of the model, and Bruce Bills and Herb Frey for discussions regarding the interpretation of the field. Finally, we thank Dave Rowlands, Despina Pavlis, Scott Luthcke, and John McCarthy for their analysis with the GEODYN interplanetary orbit program, and Joe Chan, Doug Chinn,

Huseyin Iz, Rich Ullman, and Sheila Kapoor for analytical and computer support in the preparation of the solution and material of this document.

## REFERENCES

- Anderson, J.D., L/ Efron, and S.K. Wong, Martian mass and Earth-Moon mass from coherent S-band tracking of Mariners 6 and 7, *Science*, 167, 227-229, 1970.
- Balmino, G., B. Moynot, N. Valès, Gravity field model of Mars in spherical harmonics up to degree and order eighteen, *J. Geophys. Res.*, 87, 9735-9746, 1982.
- Banerdt, W.B., M.P. Golombek, and K.L. Tanaka, Stress and tectonics on Mars, in *Mars*, 249-297, ed. H.H. Kieffer, B.M. Jakosky, C.W. Snyder, and M.S. Matthews, Univ. Ariz. Press, Tucson, 1992.
- Banerdt, W.B., R.J. Phillips, N.H. Sleep, and R.S. Saunders, Thick shell tectonics on one-plate planets: Applications to Mars, *J. Geophys. Res.*, 87, 9723-9733, 1982.
- Bills, B.G., and A.J. Ferrari, Mars topography harmonics and geophysical implications, *J. Geophys. Res.*, 83, 3497-3508, 1978.
- Born, G.H., Mars physical parameters as determined from Mariner 9 observations of the natural satellites and Doppler tracking, *J. Geophys. Res.*, 79, 4837-4844, 1974.
- Christensen, E.J., and G. Balmino, Development and analysis of a twelfth degree and order gravity model for Mars, *J. Geophys. Res.*, 84, 7943-7953, 1979.
- Christensen, E.J., and B.G. Williams, Mars gravity field derived from Viking-1 and Viking -2: The navigation result, *J. Guid. Control*, 3, 179-183, 1979.
- Culp, R.D., and A.I. Stewart, Time-dependent model of the Martian atmosphere for use in orbit lifetime and sustenance studies, *J. Astronaut. Sci.*, 32, 329-341, 1984.
- Davies, M.E., V.K. Abalakin, J.H. Lieske, P.K. Seidelmann, A.T. Sinclair, A.M. Sinzi, B.A. Smith, and Y.S. Tjuflin, Reports of IAU Working Group on Cartographic Coordinates and Rotational Elements of the Planets and Satellites, *Celest. Mech.*, 29, 309-321, 1986.
- Davies, M.E., V.K. Abalakin, M. Bursa, G.E. Hunt, J.H. Lieske, B. Morando, R.H. Rapp, P.K. Seidelmann, A.T. Sinclair, and Y.S. Tjuflin, Report of the IAU/IAU/COSPAR working group on cartographic and rotational elements of the planets and satellites: 1988, *Celest. Mech. Dynam. Astron.*, 46, 187-204, 1989.
- Davies, M.E., R.M. Batson, S.S.C. Wu, Geodesy and cartography, in *Mars*, 321-342, ed. H.H. Kieffer, B.M. Jakosky, C.W. Snyder, and M.S. Matthews, Univ. Ariz. Press, Tucson, 1992.
- Duxbury, T.C., and J.D. Callahan, Phobos and Deimos astrometric observations from Viking, *Astron. and Astrophys.*, 201, 169-176, 1988.
- Duxbury, T.C., and J.D. Callahan, Phobos and Deimos astrometric observations from Mariner 9, *Astron. and Astrophys.*, 216, 284-293, 1989.
- Esposito, P.B., S. Demcak, and D. Roth, Gravity field determination for Mars Observer, *AIAA Report*, 621-626, 1990.

- Esposito, P.B., W.B. Banerdt, G.F. Lindal, W.L. Sjogren, M.A. Slade, B.G. Bills, and D.E. Smith, and G. Balmino, Gravity and topography, in *Mars*, 209-248, ed. H.H. Kieffer, B.M. Jakosky, C.W. Snyder, and M.S. Matthews, Univ. Ariz. Press, Tucson, 1992.
- Gapcynski, J.P., R.H. Tolson, and W.H. Michael, Jr., Mars gravity field: Combined Viking and Mariner 9 results, *J. Geophys. Res.*, *82*, 4325-4327, 1977.
- Hopfield, H.S., Tropospheric effect on electromagnetically measured range: Prediction from surface weather data, *Radio Sci.*, *6*, 357-367, 1971.
- Jordan, J.F., and J. Lorell, Mariner 9: An instrument of dynamical science, *Icarus*, *25*, 146-165, 1975.
- Kaula, W.M., *Theory of Satellite Geodesy*, 124 pp., Blaisdell, Waltham, MA, 1966.
- Lambeck, K., Comments on the gravity and topography of Mars, *J. Geophys. Res.*, *84*, 6241-6247, 1979.
- Lemoine, F.G., *Mars: The Dynamics of Orbiting Satellites and Gravity Model Development*, Ph.D. Thesis, 413 pp., University of Colorado, Boulder, 1992.
- Lerch, F.J., Optimum data weighting and error calibration for estimation of gravitational parameters, *Bullet. Geodesique*, *65*, 44-52, 1991.
- Lerch, F.J., S.M. Klosko, R.E. Laubscher, C.A. Wagner, Gravity Model Improvement Using GEOS-3 (GEM-9 and -10), *J. Geophys. Res.*, *84*, 3897-3915, 1979.
- Lerch, F.J., J.G. Marsh, S.M. Klosko, E.C. Pavlis, G.B. Patel, D.S. Chinn, and C.A. Wagner, An Improved Error Assessment for the GEM-T1 Gravitational Model, *NASA Tech. Memo 100713*, Greenbelt, MD, 1988.
- Lerch, F.J., D.E. Smith, J.C. Chan, D.S. Chinn, and G.B. Patel, High Degree Gravitational Sensitivity from Mars Orbiters for the GMM-1 Gravity Model, *NASA Tech. Memo*, Greenbelt, MD, 1993.
- Lorell, J., G.H. Born, E.J. Christensen, J.F. Jordan, P.A. Laing, W.A. Martin, W.L. Sjogren, I.I. Shapiro, R.D. Reasenberg, and G.L. Slater, Mariner 9 celestial mechanics experiment, *Science*, *175*, 317-320, 1972.
- Lorell, J., G.H. Born, E.J. Christensen, P.B. Esposito, J.F. Jordan, P.A. Laing, W.L. Sjogren, S.K. Wong, R.D. Reasenberg, I.I. Shapiro, and G.L. Slater, Gravity field of Mars from Mariner 9 tracking data, *Icarus*, *18*, 304-316, 1973.
- Marsh, J.G., F.J. Lerch, B.H. Putney, D.C. Christodoulidis, D.E. Smith, T.L. Felsentreger, B.V. Sanchez, S. M. Klosko, E.C. Pavlis, T.V. Martin, J.W. Robbins, R.G. Williamson, O.L. Colombo, D.D. Rowlands, W.F. Eddy, N.L. Chandler, K.E. Rachlin, G.B. Patel, S. Bhati, and D.S. Chinn, A New Gravitational Model for the Earth from Satellite Tracking Data: GEM-T1, *J. Geophys. Res.*, *93*, B6, pp. 6169-6215, 1988.
- Marsh, J.G., F.J. Lerch, B.H. Putney, T.L. Felsentreger, B.V. Sanchez, S.M. Klosko, G.B. Patel, J.W. Robbins, R.G. Williamson, T.L. Engelis, W.F. Eddy, N.L. Chandler, D.S. Chinn, S. Kapoor, K.E. Rachin, L.E. Braatz, and E.C. Pavlis, The GEM-T2 gravitational model, *J. Geophys. Res.*, *95*, 22043-22071, 1990.
- Moritz, H., Least squares collocation, *Rev. Geophys.*, *16*, 421-430, 1978.
- Moyer, T.D., mathematical formulation of the Double Precision Orbit Determination Program (DPODP), *JPL Tech. Rept. 32-1527*, Jet Propulsion Laboratory, Pasadena, 1971.

- Nerem, R.S., J. McNamee, and B.G. Bills, A high resolution gravity model for Venus: VGM-1, *Geophys. Res. Lett.*, in press, 1993.
- Null, G.W., A solution for the mass and dynamical oblateness of Mars using Mariner IV Doppler data, *Bull. Am. Astron. Soc.* 356, 1969.
- O'Neill, W.J., J.F. Jordan, J.W. Zielenbach, S.K. Wong, R.T. Mitchell, W.A. Webb, and P.E. Koskela, *JPL Tech. Rept. 32-1586*, Jet Propulsion Laboratory, Pasadena, 1973.
- Phillips, R.J., and R.S. Saunders, The isostatic state of martian topography, *J. Geophys. Res.*, 80, 2893-2898, 1975.
- Phillips, R.J., and K. Lambeck, Gravity fields of the terrestrial planets: Long wavelength anomalies and tectonics, *Rev. Geophys.*, 18, 27-86, 1980.
- Phillips, R.J., The geophysical signature of the martian dichotomy, *EOS Trans. Am. Geophys. Un.*, 69, 389, 1988.
- Putney, B.H., General theory for dynamic satellite geodesy, The National Geodetic Satellite Program, *NASA Spec. Publ., SP-365*, 319-334, 1977.
- Reasenberg, R.D., I.I. Shapiro, and R.D. White, The gravity field of Mars, *Geophys. Res. Lett.*, 2, 89-92, 1975.
- Reasenberg, R.D., The moment of inertia and isostasy of Mars, *J. Geophys. Res.*, 82, 369-375, 1977.
- Rosborough, G.W., Satellite Orbit Perturbations Due to the Geopotential, *University of Texas, Center for Space Research Report CSR-86-1*, January, 1986.
- Rosborough, G.W., and F.G. Lemoine, Sensitivity studies of Mars orbiters for Mars gravity recovery, *J. Astron. Sci.*, 39, 327-358, 1991.
- Schwartz, K.P., Least-squares collocation for large systems, *Bull. Geod. Sci.*, 35, 309-324, 1976.
- Schwartz, K.P., On the application of least-squares collocation models to physical geodesy, in *Approximation Methods in Geodesy*, edited by H. Moritz and H. Sunkel, 89-116, H. Wichmann-Verlag, Karlsruhe, 1978.
- Sleep, N.H., and R.J. Phillips, An isostatic model for the Tharsis province, Mars, *Geophys. Res. Lett.*, 6, 803-806, 1979.
- Sleep, and R.J. Phillips, Gravity and lithospheric stress on the terrestrial planets with reference to the Tharsis region of Mars, *J. Geophys. Res.*, 90, 4469-4489, 1985.
- Sjogren, W.L., J. Lorell, L. Wong, and W. Downs, Mars gravity field based on a short arc technique, *J. Geophys. Res.*, 80, 2899-2908, 1975.
- Smith, D.E., F.J. Lerch, R.S. Nerem, G.B. Patel, and S.K. Fricke, Developing an improved higher resolution gravity field model for Mars, *EOS Trans. Am. Geophys. Un.*, 71, 1427, 1990a.
- Smith, D.E., F.J. Lerch, J.C. Chan, D.S. Chinn, H.B. Iz, A. Mallama, and G.B. Patel, Mars gravity field error analysis from simulated tracking of Mars Observer, *J. Geophys. Res.*, 95, 14155-14167, 1990b.



- Snyder, C.W., The missions of the Viking orbiters, *J. Geophys. Res.*, 82, 3971-3983, 1977.
- Snyder, C.W., The extended mission of Viking, *J. Geophys. Res.*, 84, 7917-7933, 1979.
- Standish, E.M. Jr., M.S.W. Keesey, and X.X. Newhall, JPL Development Ephemeris No. 96, *JPL Tech. Rept. 32-1603*, Jet Propulsion Laboratory, Pasadena, 1976.
- Tyler, G.L., G. Balmino, D. Hinson, W.L. Sjogren, D.E. Smith, R.T. Woo, S. Asmar, M.J. Connally, and R.A. Simpson, Radio science investigations with Mars Observer, *J. Geophys. Res.*, 97, 7759-7779, 1992.
- Willemann, R.J., and D.L. Turcotte, The role of membrane stress in the support of the Tharsis rise, *J. Geophys. Res.*, 87, 9793-9801, 1982.
- Wu, S.S.C., R. Jordan, and F.J. Schaefer, Mars global topographic map 1:15,000,000 scale, *NASA Tech. Memo. 88383*, 614-617, 1986.
- Zuber, M.T., D.E. Smith, F.J. Lerch, R.S. Nerem, G.B. Patel, and S.K. Fricke, A 40<sup>th</sup> degree and order gravitational field model for Mars, *Lunar Planet. Sci. Conf. XXII*, 1581-1582, Lunar Planet. Inst., Houston, 1991a.
- Zuber, M.T., D.E. Smith, S.C. Solomon, D.O. Muhleman, J.W. Head, J.B. Garvin, H.V. Frey, J.B. Abshire, and J.L. Bufton, The Mars Observer Laser Altimeter investigation, *J. Geophys. Res.*, 97, 7781-7797, 1992.

---

F.G. Lemoine, F.J. Lerch, R.S. Nerem, and D.E. Smith, Laboratory for Terrestrial Physics, NASA/Goddard Space Flight Center, Greenbelt, MD 20771.

M.T. Zuber, Department of Earth and Planetary Sciences, Johns Hopkins University, Baltimore, MD 21218.

G.B. Patel, Hughes-STX Corporation, Lanham, MD 20706.

S.K. Fricke, RMS Technologies, Inc., Landover, MD 20785.



**Appendix A GMM-1 Normalized Coefficients for Bombs**  
Units of  $10^{10}$

Index N M	Value	Index N M	Value	Index N M	Value	Index N M	Value	Index N M	Value	Index N M	Value
2 0	-8759770	3 0	-119062	4 0	51491	5 0	-17635	6 0	13340	7 0	13025
8 0	1075	9 0	-1924	10 0	7098	11 0	-4064	12 0	1038	13 0	-7098
14 0	1627	15 0	3462	16 0	2885	17 0	1112	18 0	-4292	19 0	-367
20 0	932	21 0	-1254	22 0	1274	23 0	395	24 0	-927	25 0	603
26 0	-417	27 0	-572	28 0	611	29 0	-73	30 0	-23	31 0	289
32 0	-303	33 0	-57	34 0	107	35 0	-129	36 0	129	37 0	72
38 0	-103	39 0	44	40 0	-34	41 0	-50	42 0	66	43 0	-10
44 0	-2	45 0	32	46 0	-36	47 0	-5	48 0	13	49 0	-17
50 0	15										

**GMM-1 Normalized Coefficients**  
Units of  $10^{10}$

Index N M	Value	Index N M	Value	Index N M	Value	Index N M	Value
2 1	36	65	2 2	-846829	490611	3 3	351325 255554
3 1	37473	252926	3 2	-159844	83160	4 3	64742 -1728
4 1	42612	37090	4 2	-10546	-89776	5 3	33602 3147
5 1	6140	20365	5 2	-41571	-12689	6 3	8376 2989
5 5	-44655	37260	6 2	8244	16668	7 3	11115 -3998
6 1	18281	-14489	6 6	27894	8686	7 7	4224 -17858
6 5	16382	16726	7 2	29707	-5593	8 3	-14824 -14281
7 1	13088	-1926	7 6	-5563	-19244	8 7	-5040 16982
7 5	-1266	-12343	8 2	15193	6245	9 3	-8436 -9009
8 1	-178	5158	8 6	-9586	-18195	9 7	-4347 8088
8 5	-29578	-17748	9 2	12058	1543	10 3	-7646 3178
9 1	2743	-439	9 6	8637	4988	10 7	2874 -5952
9 5	-20839	-14007	10 2	475	-9821	10 8	-18250 -214
9 9	-11064	-6448	10 6	6192	12122	11 3	-8925 8530
10 1	11266	-4987	10 10	-3370	8017	11 7	7927 -7097
10 5	2582	-12538	11 2	-2557	-11720	11 11	-513 -2883
10 9	-15370	-15510	11 6	-1785	-228	12 3	-14660 1901
11 1	-11144	3564	12 2	-29	8259	12 7	1595 -5631
11 5	14309	11617	12 6	-3514	-16113	12 11	7044 -15713
11 9	-3755	-3912	12 10	5315	12839	13 3	1764 3878
12 1	-11655	-4769	13 2	-469	2873	13 7	-5332 5169
12 5	6147	3962	13 6	-196	-7846	13 11	8870 -8478
12 9	6846	3922	13 10	403	-7620	14 3	5749 1038
13 1	-1541	5749	14 2	8078	-5192	14 7	-6641 1808
13 5	15	-1555	14 6	-507	-797	14 11	-8531 1998
13 9	9134	9571	14 10	-2433	-13363	15 3	-3327 -2122
13 13	3215	9523	14 14	1212	-8491	15 7	8499 3714
14 1	3403	4961	15 2	-2598	-5447	15 11	-7197 6605
14 5	-1812	-8041	15 6	-1913	4891	15 15	-4849 2455
14 9	3125	8702	15 10	-127	-4057	16 3	-2155 3452
14 13	9560	21239	15 14	-267	-11150	16 7	4516 2623
15 1	4884	-1130	16 2	-4860	-1966	16 11	-780 -6243
15 5	-10076	-3830	16 6	3250	862	16 15	-4941 1661
15 9	-2844	-1616	16 10	-5903	3735	17 3	-821 2035
15 13	-780	7182	16 14	-74	-9887	17 7	2686 -1516
16 1	-1952	-1748	17 2	1094	3650	17 11	4904 2276
16 5	-4603	3784	17 6	5287	-3206	17 15	-5352 2974
16 9	-3031	-9907	17 10	-3407	3532	18 3	823 -2615
16 13	-47	-5937	17 14	-3784	-4601	18 7	-3103 1644
17 1	-1891	-6095	18 2	-2322	3176	18 11	2969 -2634
17 5	5100	3698	18 6	1470	-4761	18 15	2471 8800
17 9	-2758	-1126	18 10	4920	663	18 16	6505 3824
17 13	-2304	-5787	18 14	-4524	-135	19 3	916 -744
17 17	1294	3664	18 18	4125	3926	19 4	-1221 1072
18 1	928	-1651	19 2	-2009	-354		
18 5	2770	-2105					
18 9	-659	2574					
18 13	-2052	-2866					
18 17	-2537	-10316					
19 1	-356	3177					

19 5	-656	-4842	19 6	-2357	-356	19 7	-2816	1916	19 8	2104	-1229
19 9	1811	1296	19 10	4991	-2701	19 11	-1794	-2998	19 12	-2241	-509
19 13	-2319	-51	19 14	1528	3316	19 15	6693	5066	19 16	120	67
19 17	-1400	-5709	19 18	-3755	5285	19 19	-4330	-7073			
20 1	495	471	20 2	1354	-70	20 3	-13	1344	20 4	-3172	1197
20 5	1081	655	20 6	-767	3421	20 7	2017	-216	20 8	504	-1005
20 9	412	-412	20 10	-3443	-1056	20 11	371	-793	20 12	-2697	-352
20 13	733	1170	20 14	4163	993	20 15	2649	-2346	20 16	2587	-3006
20 17	-1456	-3704	20 18	-1467	4563	20 19	3390	-3203	20 20	-2683	-1003
21 1	-325	968	21 2	354	-941	21 3	1197	362	21 4	765	-1528
21 5	1335	1547	21 6	314	357	21 7	120	-1014	21 8	1066	867
21 9	-1138	-1707	21 10	-3759	1474	21 11	-1400	-1018	21 12	1336	1875
21 13	879	-365	21 14	2449	-1119	21 15	-2626	-3741	21 16	-1381	-977
21 17	-891	-4056	21 18	1246	4204	21 19	2056	-3136	21 20	-3203	-1656
21 21	5804	3508									
22 1	-1017	629	22 2	425	-942	22 3	-916	116	22 4	-493	-1702
22 5	-498	-291	22 6	-983	-750	22 7	363	-129	22 8	-2045	-367
22 9	-708	285	22 10	-420	1760	22 11	1768	978	22 12	159	1274
22 13	207	-575	22 14	302	-2859	22 15	-3032	1641	22 16	-2003	559
22 17	-134	2182	22 18	-2327	2049	22 19	4199	-2721	22 20	-3654	-760
22 21	3178	4536	22 22	-2939	-4231						
23 1	797	-1320	23 2	904	1211	23 3	-976	164	23 4	284	1012
23 5	-813	1652	23 6	893	-209	23 7	555	525	23 8	-877	-888
23 9	-24	613	23 10	-495	-588	23 11	3431	-453	23 12	370	-1587
23 13	172	19	23 14	-999	-1083	23 15	-1586	3652	23 16	1270	3183
23 17	2590	3795	23 18	1305	-1419	23 19	2731	-251	23 20	-3323	-2219
23 21	93	5393	23 22	289	-3163	23 23	-4795	3801			
24 1	266	28	24 2	-558	2	24 3	1161	-803	24 4	1584	34
24 5	-287	133	24 6	922	-1019	24 7	-1622	314	24 8	952	618
24 9	-282	367	24 10	361	-1484	24 11	-1107	-499	24 12	-754	-1070
24 13	-439	37	24 14	-263	2400	24 15	1938	1017	24 16	3406	1024
24 17	3062	-1506	24 18	172	-2146	24 19	141	-172	24 20	-1456	-1875
24 21	-1393	3572	24 22	857	-3239	24 23	-3123	467	24 24	3881	421
25 1	-288	-101	25 2	-730	-643	25 3	-507	-234	25 4	-1082	102
25 5	27	-1263	25 6	-812	309	25 7	33	360	25 8	471	473
25 9	431	547	25 10	569	-435	25 11	-37	1177	25 12	-1449	596
25 13	753	870	25 14	1893	1141	25 15	1177	-1792	25 16	24	-1280
25 17	-1941	-3299	25 18	-679	-830	25 19	-1831	-48	25 20	-217	-364
25 21	-2267	2070	25 22	1882	-1612	25 23	-3209	1229	25 24	2935	461
25 25	-225	-4911									
26 1	193	-584	26 2	-22	652	26 3	-225	734	26 4	-370	1013
26 5	421	464	26 6	111	632	26 7	896	-44	26 8	783	-653
26 9	267	-968	26 10	-95	-110	26 11	777	-280	26 12	771	300
26 13	443	-415	26 14	873	-541	26 15	-1253	-889	26 16	-1576	373
26 17	-1821	950	26 18	-1007	1766	26 19	202	721	26 20	147	1522
26 21	-1150	-483	26 22	1568	-320	26 23	-2330	-1304	26 24	2540	673
26 25	99	-2899	26 26	-1192	5301						
27 1	-235	724	27 2	-71	-83	27 3	894	-20	27 4	778	-669
27 5	313	-93	27 6	55	-423	27 7	-480	-384	27 8	-128	-65
27 9	-661	-564	27 10	152	-68	27 11	-1040	-614	27 12	426	73
27 13	-512	-614	27 14	-346	671	27 15	-350	243	27 16	151	830
27 17	1184	1412	27 18	826	1173	27 19	1432	1371	27 20	1259	-637
27 21	-17	-520	27 22	-272	-198	27 23	-854	-1218	27 24	738	1055
27 25	352	-1928	27 26	-1735	2172	27 27	3652	-1478			
28 1	-12	259	28 2	217	-235	28 3	-553	-141	28 4	-642	-400
28 5	-90	-363	28 6	-389	200	28 7	93	-15	28 8	-550	226
28 9	66	353	28 10	-192	205	28 11	-29	439	28 12	-424	311
28 13	222	507	28 14	441	33	28 15	-462	-153	28 16	183	-268
28 17	1052	-7	28 18	968	-1135	28 19	1950	-913	28 20	-159	-1609
28 21	-765	-1283	28 22	-922	-227	28 23	-189	-112	28 24	67	480
28 25	985	-563	28 26	-1511	1764	28 27	3156	-617	28 28	-2317	-2645
29 1	141	-229	29 2	383	340	29 3	-53	205	29 4	40	388
29 5	-142	595	29 6	389	115	29 7	131	-12	29 8	68	-246
29 9	16	-237	29 10	-154	171	29 11	479	202	29 12	417	-122
29 13	148	-275	29 14	-441	-353	29 15	-427	820	29 16	-153	168
29 17	356	-678	29 18	-901	-842	29 19	-929	-1161	29 20	-1499	-617
29 21	-1114	399	29 22	-550	707	29 23	798	456	29 24	608	-113
29 25	563	442	29 26	-1514	299	29 27	2376	318	29 28	108	-1447
29 29	-1280	785									

30 1	-167	253	30 2	-69	-288	30 3	380	-260	30 4	410	-421
30 5	-88	-1	30 6	7	-346	30 7	-431	15	30 8	-195	275
30 9	-276	243	30 10	318	-81	30 11	-22	-156	30 12	-156	-431
30 13	-192	1	30 14	-638	774	30 15	1077	291	30 16	248	86
30 17	-629	-481	30 18	-766	789	30 19	-1698	1288	30 20	153	1163
30 21	-183	927	30 22	1178	130	30 23	486	-619	30 24	231	-839
30 25	-127	189	30 26	-500	-109	30 27	1175	737	30 28	-416	-740
30 29	-225	802	30 30	310	-1096						
31 1	127	-271	31 2	-99	-98	31 3	-533	-65	31 4	-401	117
31 5	-52	-134	31 6	-195	157	31 7	222	184	31 8	82	200
31 9	458	262	31 10	-131	-151	31 11	89	56	31 12	-587	-33
31 13	256	599	31 14	625	145	31 15	39	-1017	31 16	-159	-395
31 17	-529	847	31 18	796	659	31 19	1177	1207	31 20	1324	84
31 21	911	-172	31 22	163	-1061	31 23	-424	-960	31 24	-376	59
31 25	-448	251	31 26	-478	17	31 27	488	581	31 28	250	-853
31 29	-476	531	31 30	850	-224	31 31	159	708			
32 1	34	-257	32 2	-31	248	32 3	159	209	32 4	215	382
32 5	17	190	32 6	213	-11	32 7	135	-33	32 8	285	-345
32 9	41	-338	32 10	-62	9	32 11	21	173	32 12	265	224
32 13	126	-219	32 14	-60	-368	32 15	-775	152	32 16	-257	254
32 17	836	318	32 18	458	-703	32 19	888	-951	32 20	31	-1123
32 21	-190	-1028	32 22	-752	-345	32 23	-510	609	32 24	-26	569
32 25	-84	262	32 26	-215	-50	32 27	351	346	32 28	226	-300
32 29	-303	38	32 30	434	-77	32 31	-531	671	32 32	-390	-1122
33 1	-112	241	33 2	-158	-154	33 3	261	-122	33 4	168	-261
33 5	44	-225	33 6	-107	-126	33 7	-204	-43	33 8	-109	78
33 9	-229	96	33 10	240	-22	33 11	15	-142	33 12	178	-72
33 13	-115	-70	33 14	-333	275	33 15	318	378	33 16	350	134
33 17	77	-627	33 18	-765	-369	33 19	-1078	-477	33 20	-690	54
33 21	-926	-10	33 22	-336	602	33 23	540	292	33 24	600	219
33 25	128	-192	33 26	-104	-60	33 27	123	257	33 28	57	-373
33 29	-189	1	33 30	466	267	33 31	-686	79	33 32	314	-194
33 33	-1315	309									
34 1	118	-47	34 2	33	55	34 3	-297	34	34 4	-331	85
34 5	35	-78	34 6	-54	196	34 7	140	12	34 8	78	63
34 9	202	-4	34 10	-129	-47	34 11	-136	-101	34 12	-129	-50
34 13	-28	158	34 14	416	-48	34 15	5	-447	34 16	81	-379
34 17	-628	244	34 18	-94	619	34 19	-53	945	34 20	51	517
34 21	81	699	34 22	547	246	34 23	454	-240	34 24	137	-530
34 25	-193	-211	34 26	52	-269	34 27	-19	-6	34 28	132	-70
34 29	-52	47	34 30	110	264	34 31	-469	-210	34 32	159	94
34 33	-900	-687	34 34	1397	580						
35 1	-55	22	35 2	98	124	35 3	194	113	35 4	138	69
35 5	16	145	35 6	135	-28	35 7	-19	-99	35 8	4	-168
35 9	-179	-211	35 10	-2	120	35 11	-107	162	35 12	164	139
35 13	-99	-209	35 14	-204	-269	35 15	-317	181	35 16	-300	110
35 17	322	329	35 18	491	-66	35 19	739	-171	35 20	350	-87
35 21	433	-86	35 22	465	-510	35 23	-166	-224	35 24	-430	-118
35 25	-264	97	35 26	-97	-241	35 27	-282	118	35 28	159	26
35 29	-90	-33	35 30	129	273	35 31	-283	-269	35 32	22	248
35 33	-395	-731	35 34	-61	924	35 35	747	-407			
36 1	-60	179	36 2	-12	-151	36 3	41	-121	36 4	29	-252
36 5	0	-60	36 6	-97	-69	36 7	-125	21	36 8	-190	174
36 9	-107	178	36 10	131	14	36 11	138	-95	36 12	-12	-111
36 13	-22	98	36 14	-289	253	36 15	319	222	36 16	109	224
36 17	156	-295	36 18	-194	-343	36 19	-500	-519	36 20	1	-142
36 21	0	-349	36 22	-379	-387	36 23	-267	70	36 24	-77	360
36 25	200	217	36 26	-178	95	36 27	-35	251	36 28	242	25
36 29	6	-119	36 30	-63	247	36 31	-111	-176	36 32	-105	189
36 33	-86	-664	36 34	-286	234	36 35	608	60	36 36	-602	257
37 1	93	-129	37 2	66	33	37 3	-225	17	37 4	-154	96
37 5	-31	55	37 6	8	69	37 7	110	59	37 8	76	30
37 9	227	8	37 10	-152	-64	37 11	-73	-28	37 12	-179	-43
37 13	89	113	37 14	297	74	37 15	94	-310	37 16	113	-150
37 17	-276	-4	37 18	-119	277	37 19	-202	548	37 20	-72	39
37 21	-214	-61	37 22	-289	307	37 23	47	333	37 24	338	101
37 25	135	-212	37 26	202	114	37 27	174	-89	37 28	102	-69
37 29	-109	-98	37 30	-31	142	37 31	17	-226	37 32	-162	77
37 33	185	-490	37 34	-275	88	37 35	402	286	37 36	-584	-487

37 37	113	405									
38 1	-58	-57	38 2	-4	28	38 3	145	28	38 4	168	59
38 5	-32	64	38 6	56	-74	38 7	-20	-17	38 8	10	-126
38 9	-88	-70	38 10	10	61	38 11	25	170	38 12	79	140
38 13	17	-124	38 14	-95	-161	38 15	-161	46	38 16	-157	-3
38 17	122	113	38 18	208	-13	38 19	492	-16	38 20	12	-16
38 21	-85	125	38 22	300	293	38 23	226	-66	38 24	84	-223
38 25	-205	-176	38 26	112	-231	38 27	-127	-200	38 28	-76	15
38 29	-7	21	38 30	-200	60	38 31	21	-82	38 32	-146	10
38 33	253	-265	38 34	-239	-102	38 35	175	386	38 36	-165	-558
38 37	103	393	38 38	-293	-236						
39 1	3	50	39 2	-86	-79	39 3	-18	-73	39 4	-10	-78
39 5	6	-92	39 6	-68	-7	39 7	-31	36	39 8	-40	98
39 9	9	122	39 10	81	-34	39 11	156	-111	39 12	26	-98
39 13	13	73	39 14	-91	100	39 15	64	85	39 16	56	88
39 17	14	-91	39 18	-114	-182	39 19	-252	-336	39 20	-19	15
39 21	172	62	39 22	197	-247	39 23	-64	-185	39 24	-205	-46
39 25	-87	162	39 26	-216	-63	39 27	-168	59	39 28	33	135
39 29	67	-49	39 30	-106	80	39 31	39	-2	39 32	-66	-117
39 33	236	-134	39 34	-78	-161	39 35	26	372	39 36	19	-472
39 37	-87	355	39 38	63	-446	39 39	72	-543			
40 1	58	-74	40 2	15	67	40 3	-79	57	40 4	-89	110
40 5	8	5	40 6	35	64	40 7	72	-13	40 8	109	-41
40 9	110	-68	40 10	-83	-49	40 11	-139	-32	40 12	-60	-25
40 13	-10	-5	40 14	199	-23	40 15	-28	-119	40 16	73	-93
40 17	-122	40	40 18	-70	169	40 19	-96	311	40 20	12	21
40 21	31	-162	40 22	-207	-129	40 23	-124	96	40 24	15	190
40 25	104	25	40 26	21	171	40 27	91	100	40 28	75	27
40 29	-2	-54	40 30	-67	70	40 31	134	-56	40 32	-79	-63
40 33	107	20	40 34	-57	-76	40 35	-110	235	40 36	142	-403
40 37	-118	212	40 38	195	-243	40 39	221	76	40 40	-83	105
41 1	-61	38	41 2	-4	9	41 3	129	18	41 4	94	-15
41 5	11	9	41 6	14	-31	41 7	-47	-47	41 8	-30	-66
41 9	-135	-52	41 10	51	64	41 11	-10	93	41 12	78	96
41 13	-53	-72	41 14	-123	-127	41 15	-67	85	41 16	-100	-14
41 17	91	56	41 18	130	-12	41 19	284	-71	41 20	-6	-42
41 21	-153	18	41 22	-35	213	41 23	65	36	41 24	122	-47
41 25	23	-85	41 26	156	-55	41 27	59	-72	41 28	25	-35
41 29	-12	28	41 30	27	-67	41 31	46	-66	41 32	-51	-48
41 33	147	58	41 34	75	-86	41 35	-117	125	41 36	180	-199
41 37	-131	132	41 38	226	-113	41 39	-37	32	41 40	56	60
41 41	37	-121									
42 1	17	63	42 2	-10	-40	42 3	-52	-38	42 4	-54	-75
42 5	20	-37	42 6	-38	11	42 7	-16	20	42 8	-46	97
42 9	9	65	42 10	36	-19	42 11	62	-100	42 12	1	-88
42 13	-4	79	42 14	-55	98	42 15	60	43	42 16	29	71
42 17	6	-53	42 18	-46	-104	42 19	-231	-193	42 20	-13	66
42 21	88	128	42 22	166	-39	42 23	-6	-43	42 24	-77	-77
42 25	-38	15	42 26	-62	-93	42 27	-47	-23	42 28	-26	-27
42 29	60	-2	42 30	-94	-87	42 31	-44	-23	42 32	-33	6
42 33	162	18	42 34	-5	-89	42 35	-154	34	42 36	122	-128
42 37	-102	69	42 38	211	5	42 39	19	17	42 40	50	134
42 41	-64	-144	42 42	140	9						
43 1	20	-42	43 2	52	42	43 3	-37	37	43 4	-36	49
43 5	-10	40	43 6	31	13	43 7	35	-4	43 8	41	-31
43 9	51	-47	43 10	-68	-14	43 11	-117	23	43 12	-59	14
43 13	8	-19	43 14	117	17	43 15	26	-71	43 16	45	-35
43 17	-46	-1	43 18	-42	96	43 19	-36	252	43 20	79	-2
43 21	71	-114	43 22	-84	-112	43 23	-33	40	43 24	-17	104
43 25	27	-8	43 26	-24	71	43 27	11	16	43 28	-40	24
43 29	-35	-12	43 30	-96	15	43 31	17	145	43 32	29	-31
43 33	37	-20	43 34	-31	-71	43 35	-64	61	43 36	139	-42
43 37	-44	45	43 38	152	45	43 39	-29	32	43 40	-3	117
43 41	15	-209	43 42	83	174	43 43	-37	-33			
44 1	-42	15	44 2	-7	-19	44 3	65	-17	44 4	73	-29
44 5	-11	12	44 6	-8	-33	44 7	-34	0	44 8	-45	-23
44 9	-72	8	44 10	30	47	44 11	65	71	44 12	38	70
44 13	7	-27	44 14	-81	-56	44 15	-13	22	44 16	-59	-7
44 17	34	15	44 18	74	-11	44 19	205	-60	44 20	-26	-102

44 21	-127	-14	44 22	-46	124	44 23	50	-9	44 24	70	-20
44 25	-16	-37	44 26	62	-7	44 27	-12	-35	44 28	15	55
44 29	7	45	44 30	30	55	44 31	138	12	44 32	8	-72
44 33	-27	71	44 34	-7	40	44 35	-55	-2	44 36	76	-61
44 37	-54	25	44 38	90	41	44 39	-25	12	44 40	-25	117
44 41	46	-142	44 42	-12	177	44 43	116	-108	44 44	54	186
45 1	31	1	45 2	-16	-21	45 3	-57	-26	45 4	-39	-14
45 5	0	-20	45 6	-16	9	45 7	14	26	45 8	-3	57
45 9	56	46	45 10	0	-32	45 11	59	-74	45 12	-8	-76
45 13	22	44	45 14	9	67	45 15	3	-3	45 16	20	46
45 17	-11	-18	45 18	-27	-60	45 19	-149	-127	45 20	-71	72
45 21	45	100	45 22	108	-18	45 23	-27	-46	45 24	-47	-41
45 25	-40	41	45 26	-36	-35	45 27	-27	30	45 28	48	-5
45 29	60	-21	45 30	44	-58	45 31	4	-95	45 32	-51	-41
45 33	45	123	45 34	92	0	45 35	-45	-17	45 36	73	6
45 37	-35	26	45 38	52	54	45 39	-34	34	45 40	-57	84
45 41	65	-121	45 42	-53	132	45 43	152	12	45 44	-81	171
45 45	11	-12									
46 1	2	-42	46 2	13	26	46 3	4	30	46 4	0	52
46 5	-10	15	46 6	21	4	46 7	21	-14	46 8	42	-46
46 9	25	-36	46 10	-33	-9	46 11	-77	30	46 12	-29	23
46 13	-3	-36	46 14	67	-22	46 15	-2	-23	46 16	27	-33
46 17	-13	1	46 18	-38	52	46 19	-2	154	46 20	66	28
46 21	58	-78	46 22	-61	-70	46 23	-36	38	46 24	-3	64
46 25	49	22	46 26	3	50	46 27	42	15	46 28	-10	-36
46 29	-55	-39	46 30	-37	-66	46 31	-85	33	46 32	-15	35
46 33	72	-5	46 34	41	-87	46 35	-81	-19	46 36	82	11
46 37	-46	-2	46 38	29	52	46 39	-32	8	46 40	-46	51
46 41	76	-72	46 42	-73	81	46 43	102	47	46 44	-139	85
46 45	14	47	46 46	-100	20						
47 1	-24	19	47 2	-24	-14	47 3	40	-12	47 4	39	-20
47 5	5	-11	47 6	-11	-8	47 7	-26	-3	47 8	-22	-7
47 9	-53	6	47 10	37	26	47 11	54	21	47 12	39	30
47 13	-10	-1	47 14	-69	-50	47 15	-17	27	47 16	-38	-16
47 17	11	10	47 18	41	-2	47 19	112	-62	47 20	-10	-67
47 21	-90	-11	47 22	-23	87	47 23	49	9	47 24	46	-33
47 25	11	-45	47 26	45	-22	47 27	3	-37	47 28	-39	15
47 29	-9	60	47 30	-44	22	47 31	20	79	47 32	38	8
47 33	-25	-20	47 34	-91	-20	47 35	-19	31	47 36	45	2
47 37	-29	-7	47 38	21	53	47 39	-30	-1	47 40	-47	35
47 41	57	-48	47 42	-66	46	47 43	65	76	47 44	-134	9
47 45	-40	55	47 46	-86	-48	47 47	133	76			
48 1	27	9	48 2	-1	1	48 3	-38	-2	48 4	-41	-4
48 5	11	-14	48 6	0	14	48 7	11	4	48 8	8	36
48 9	32	10	48 10	-3	-25	48 11	-4	-57	48 12	-6	-60
48 13	-3	28	48 14	15	45	48 15	-2	3	48 16	12	31
48 17	-5	0	48 18	-10	-27	48 19	-109	-63	48 20	-39	61
48 21	39	73	48 22	74	-27	48 23	-7	-39	48 24	-48	-26
48 25	-41	8	48 26	-40	-25	48 27	-19	16	48 28	22	26
48 29	60	0	48 30	22	13	48 31	44	3	48 32	24	-38
48 33	-42	41	48 34	4	91	48 35	32	-22	48 36	30	12
48 37	-21	-15	48 38	0	31	48 39	-21	-7	48 40	-44	18
48 41	55	-34	48 42	-55	29	48 43	26	67	48 44	-97	-22
48 45	-55	36	48 46	-38	-75	48 47	1	137	48 48	54	40
49 1	-10	-8	49 2	18	16	49 3	18	21	49 4	5	17
49 5	-3	14	49 6	10	-2	49 7	1	-14	49 8	12	-31
49 9	-9	-26	49 10	-12	6	49 11	-63	36	49 12	-18	34
49 13	-8	-26	49 14	26	-15	49 15	17	-5	49 16	15	-20
49 17	4	-2	49 18	-18	29	49 19	14	109	49 20	66	-4
49 21	40	-58	49 22	-53	-47	49 23	-29	25	49 24	-8	55
49 25	24	23	49 26	2	47	49 27	26	0	49 28	9	-26
49 29	-28	-52	49 30	13	-13	49 31	-1	-21	49 32	-19	-24
49 33	11	33	49 34	81	-4	49 35	-11	-52	49 36	-3	17
49 37	-18	-6	49 38	-16	34	49 39	-3	-14	49 40	-35	13
49 41	41	-15	49 42	-52	19	49 43	11	46	49 44	-77	-37
49 45	-61	1	49 46	8	-63	49 47	-41	57	49 48	-31	49
49 49	-6	114									
50 1	-11	20	50 2	-8	-14	50 3	11	-16	50 4	18	-27
50 5	3	-2	50 6	-11	-6	50 7	-17	8	50 8	-27	10

50 9	-28	12	50 10	18	17	50 11	51	6	50 12	23	13
50 13	5	11	50 14	-42	-12	50 15	-3	4	50 16	-23	-3
50 17	1	2	50 18	32	-4	50 19	64	-50	50 20	-25	-60
50 21	-67	-5	50 22	-12	65	50 23	34	10	50 24	42	-15
50 25	11	-29	50 26	34	-21	50 27	-15	-24	50 28	-34	0
50 29	-29	45	50 30	-1	-8	50 31	-16	0	50 32	-17	11
50 33	3	8	50 34	-10	-65	50 35	-36	-8	50 36	18	31
50 37	4	1	50 38	-1	27	50 39	-3	-14	50 40	-33	-7
50 41	39	-6	50 42	-41	3	50 43	5	35	50 44	-58	-39
50 45	-39	-11	50 46	16	-39	50 47	-42	36	50 48	-35	9
50 49	-99	41	50 50	-62	34						



**Table 1. Planetary and Astronomical Constants**

Parameter	Value	Unit
Gravitational Constant (GM)	42828.28	km <sup>3</sup> s <sup>-2</sup>
Equatorial Radius of Mars	3394.2	km
Spin Rate of Mars	350.891983	deg day <sup>-1</sup>
Solid Tide Amplitude (k <sub>2</sub> )	0.05	
Flattening of Mars	1/191.1372	
Speed of Light	2.99792458x10 <sup>8</sup>	m s <sup>-1</sup>
Astronomical Unit	1.49597870660x10 <sup>11</sup>	m

**Table 2. SATELLITE ORBIT CHARACTERISTICS**  
Including Beat Periods and Ground Track Walks

Satellite	Periapsis altitude (km)	Epoch * (Yr-Mo-Da)	Inclination (degrees), Eccentricity	Orbit period (hours)	Periapsis argmnt. (*), rate (*day)	Nodal rate (*day)	Beat period (days)	Walk per revolution (degrees)	Comments
Mariner 9	1500	71-11-16	64, 0.62	11.81	-24, -0.02	-0.18	18.3	10°	New orbit
		71-12-31		11.98			19.5	End of data	
		72-04-19							
Viking 1	1500	76-06-21	38, 0.75	24.63	47, 0.17	-0.13	> 1000	< 1	Synchronous
		76-09-13		21.87	56	8	44	9 rev. near repeat	
		76-08-24		24.63	60	> 1000	< 1	Over lander	
		77-01-22		22.99	79	14	25	Near Phobos	
		77-03-12		21.92	99, 0.27	8	43	New orbit	
		77-03-24		23.50	102	21	17	New walk	
		77-07-01		23.97	120	38	10 **	Dual station	
		78-12-02		24.85	264	-129	-3	Near synch.	
		79-01-27			270			End of data	
		Viking 2		1400	76-08-07	55, 0.76	27.31	72, 0.05	-0.09
76-08-28	24.63		73		> 1000		< 1	Synchronous	
76-10-02	26.79		68, -0.05		-13		-29	New incl.	
76-12-21	26.48		62, -0.08		-15		-25	Low periaps./Incl. change	
77-03-05	24.73		55		-215		-2	Over lander	
77-04-18	22.72		51		12		29	13 rev. near repeat	
77-09-26	24.29		34		78		5	Near Deimos	
77-10-09	24.20		33		60		6	Near Deimos	
77-10-25	300		32, -0.10		39		9	Low periaps.	
			2					End of data	

\* Walk for two 12 hr. revolution for Mariner 9 orbits

\* Start epoch of the orbit parameters cited

\*\* Secondary walk is about 2 degrees over approximately 200 day duration

Table 3.  
 Summary of Data used in Mars Gravity Model GMM-1  
 DSN Tracking Data ( $\pm .1$  cm / sec)

Satellite	Altitude km.	Inclination degree	Total	ARCS			Total Number of Observations	Total No. of Days
				Average Arc-Length (days)	Average Input RMS Residuals (cm/sec)	Average No. of Obs.		
Viking-1	1500	38.2	29	4.2	.446	1,082	31,393	122
Viking-1 Sci-2	300	39.1	95	4.8	2.844	673	63,977	425
Viking-2	1400	55.4	12	3.8	.256	990	11,878	46
Viking-2	1500	75.1	11	4.7	.507	952	10,467	52
Viking-2	778	80.1	54	3.8	.210	655	35,375	204
Viking-2	300	80.2	37	4.2	6.282	793	29,355	155
Mariner-9	1500	64.4	32	4.3	.212	1,559	49,878	138
Total			270				232,323	1,142

**Table 4. HAP<sup>\*</sup> Velocity Perturbations By Degree**

USING A POWER RULE OF  $13E-05/L^{**2}$   
 MARINER 9, VIKING 1 & 2 SAMPLED ORBITS \*\*  
 VELOCITY PERTURBATIONS IN CM/SEC

PERIAPSIS ALTITUDE(KM):	VKG1 300	VKG2 300	VKG2 800	VKG1 1500	MRN9 1500
DEGREE	EPOCH 78-01-15	EPOCH 77-12-17	EPOCH 77-04-19	EPOCH 77-02-05	EPOCH 72-04-10
2	566.175	653.411	144.452	64.324	828.128
3	353.495	218.135	39.761	36.417	100.049
4	207.188	106.629	16.519	13.981	55.852
5	107.358	59.610	7.771	5.659	24.812
6	66.205	34.485	4.248	2.270	12.463
7	40.783	21.119	2.498	1.051	6.003
8	28.610	13.923	1.617	0.579	2.669
9	18.054	9.347	1.197	0.304	1.135
10	13.176	6.677	1.118	0.158	0.490
11	9.049	4.736	1.523	0.093	0.260
12	6.808	3.555	2.686	0.056	0.167
13	4.711	2.649	1.195	0.031	0.105
14	3.858	2.053	1.350	0.019	0.061
18	1.390	0.780	0.211	0.010	0.002
22	0.581	0.381	0.048	0.002	0.000
26	0.317	0.249	0.012	0.000	0.000
30	0.260	0.110	0.004	0.000	0.000
34	0.370	0.047	0.000	0.000	0.000
36	0.507	0.034	0.000	0.000	0.000
38	0.468	0.028	0.000	0.000	0.000
40	0.373	0.029	0.000	0.000	0.000
42	0.241	0.036	0.000	0.000	0.000
46	0.265	0.038	0.000	0.000	0.000
50	0.322	0.027	0.000	0.000	0.000

\* HAP: HARMONIC ANALYSIS OF PERTURBATIONS FROM ANALYTIC THEORY.

\*\* PERIODS GT. 8 DAYS HAVE THEIR AMPLITUDES MULTIPLIED BY (8/PERIOD).  
 PERIODS GT. 40 DAYS HAVE BEEN EXCLUDED.

**Table 5. Orbit Accuracy Tests : RMS of Orbital Fits in cm/sec**

Arc #	Satellite	Arc epoch yyymmdd	No. of obs.	Arc length days	Balmino 18 x 18	GMM-1 50 x 50
1	Mariner-9 inc. = 64°	720113	1896	4	.456	.090
2	VO1 1500 km. inc. = 39°	760822	1326	6	.687	.097
3	VO2 1500 km. inc. = 55°	760917	1511	6	.387	.196
4	VO2 1500 km. inc. = 75°	761026	1350	6	.649	.340
5	VO2 800 km. inc. = 80°	770102	682	4	.434	.143
Average					.522	.173
6	VO1 300 km inc. = 39°	771122	568	9	5.07	1.04
7		780210	754	9	6.44	1.22
8		780604	538	2	2.42	.74
9		780811	387	2	1.43	.09
10		780904	1025	8	8.58	1.24
Average					4.79	.87
11	VO2 300 km inc. = 80°	771117	1114	6	1.52	1.02
12		771217	688	2	.73	.11
13		780516	791	8	7.67	1.78
14		780526	705	4	.60	.15
Average					2.63	.77

For arcs 1-5 arc parameters adjusted are position, velocity,  $C_r$  and station biases  
 For arcs 6-14 arc parameters adjusted are position, velocity,  $C_r$  and  $C_d$  per arc  
 Arc 13 comes in as 2 separate arcs in GMM-1

**Table 6. Orbit Prediction Tests : RMS of Prediction Fits in cm/sec**

Arc #	Satellite	Arc epoch yyymmdd	No. of obs.	Predict ed period days	Balmino 18 x 18	GMM-1 50 x 50
1	Mariner-9 inc. = 64°	720113	1308	3	5.61	.36
2	VO1 1500 km. inc. = 39°	760822	840	3	4.20	2.58
3	VO2 1500 km. inc. = 55°	760917	720	3	1.62	.68
4	VO2 1500 km. inc. = 75°	761026	697	3	8.04	2.38
5	VO2 800 km. inc. = 80°	770102	367	3	21.40	.73
Average					8.17	1.34
6	VO1 300 km. inc. = 39°	780904	353	3	105.6	13.2
7	VO2 300 km. inc. = 80°	771117	597	3	102.9	30.1

**Table 7. Calibration and Data Weights of GMM-1**

Subset Solution Dataset Removed	Apriori Sigma Weights $\sigma_o$ cm / sec	GMM-1 Sigma Weights $\sigma_o$ cm / sec	GMM-1 Calibration Factors $k^{**}$
VO2 1500 km 55° Inc.	1.0	4.1	1.2
VO2 1500 km 75° Inc.	1.0	1.5	.81
VO2 800km 80° Inc.	.71	.72	.81
VO2 300 km 80° Inc.	.71	1.0	1.16
VO1 1500 km. 39° Inc.	1.0	3.5	.96
VO1 300 km 39° Inc	.71	.8	1.05
Mariner-9	1.0	2.0	.99

$$k = \left( \frac{\sum (c - \bar{c})^2}{\sum (\sigma^2 - \sigma^2)} \right)^{\frac{1}{2}}$$

$$w' = \frac{w}{k^2}$$

$$\sigma_o = \frac{1}{\sqrt{w}} \qquad \sigma'_o = \frac{1}{\sqrt{w'}}$$

\*\*  $k=1$  for complete convergence

**Table 8. Projected Gravity Orbit Error from GMM-1 Covariances**

( Long period terms excluded )

Orbit Position Error in meters

	Arc				
Satellite	Length (days)	Radial	Along-Track	Cross-Track	Total
Mars Observer	6	67	757	90	765
Mariner-9	6	2	4	2	5
Viking-1,300 km	6	26	69	31	80
Viking-2,300 km	6	26	83	12	87

Orbit Velocity Error in cm/sec

	Arc				
Satellite	Length (days)	Radial	Along-Track	Cross-Track	Total
Mars Observer	6	66.3	8.0	8.0	67.1
Mariner-9	6	.07	.03	.02	.08
Viking-1,300 km	6	1.9	.8	.2	2.1
Viking-2,300 km	6	2.0	.9	.1	2.3



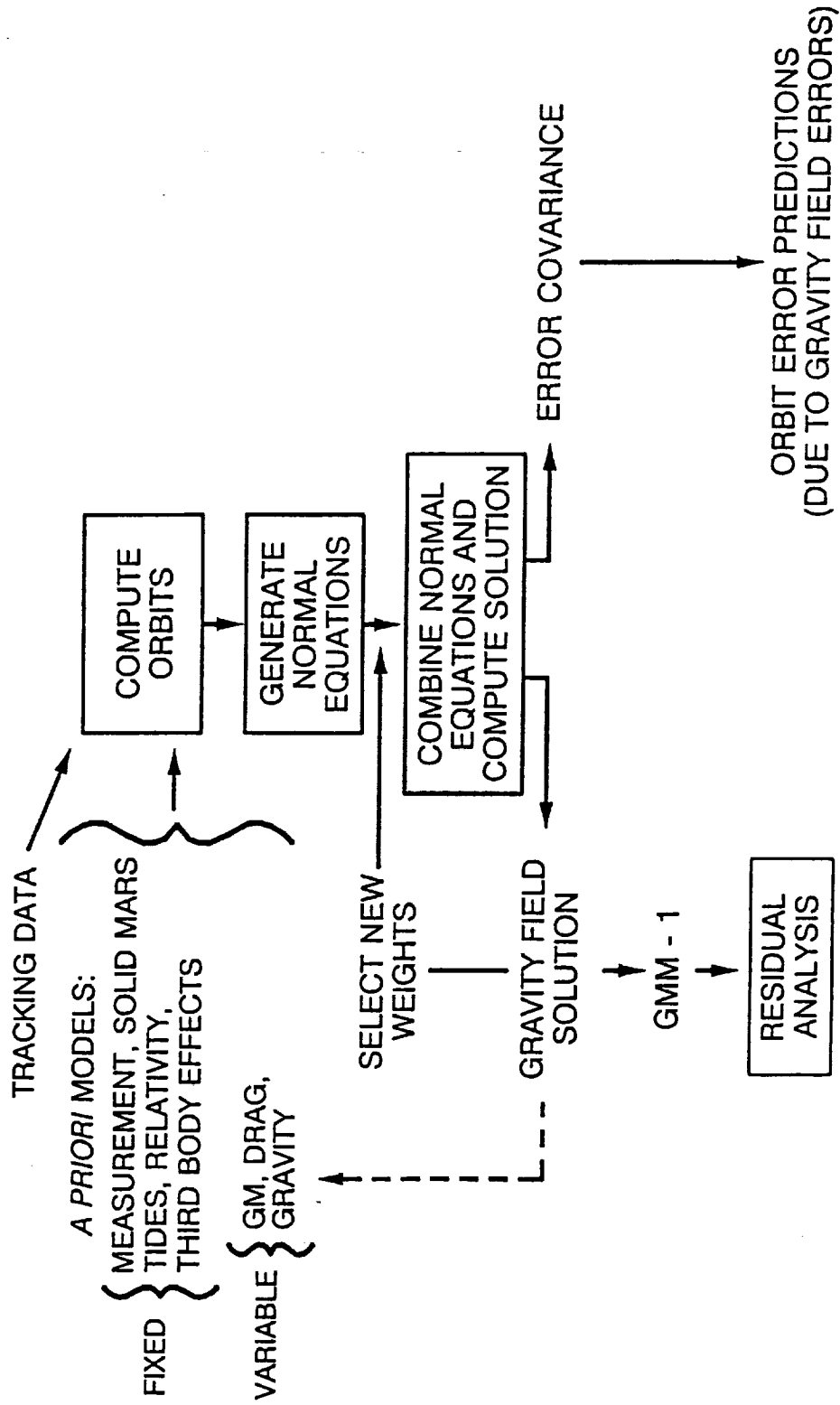
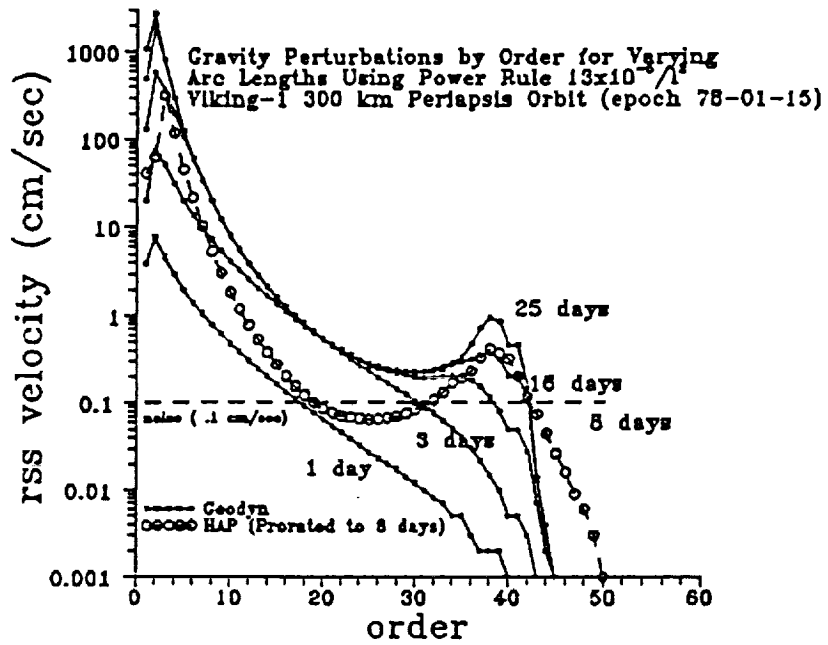


Figure 1.



- GEODYN: Numerically integrated perturbations
- HAP: Harmonic analysis of perturbations from analytical theory

Figure 2. Spectral Sensitivity of Gravity Signal (by Order)

( $\omega=175^\circ$ )

Velocity Perturbations In .001 cm/sec

RSS'	DEG	VKG1: 78-01-15
192339	2 ***	Arg. of periapsis = 175 deg
124383	6 *****	8 day arc length
28804	10 469*****	
8027	14 54*****156	
2909	18 6 52***843 28	
1297	22 3 10138592237 8	
675	26 1 2 7161289 76 3	
400	30 1 1 2 20137143 29 2	
268	34 0 0 1 2 33104 77 13 1	
229	36 0 0 0 1 13 69 86 29 2 1	
203	38 0 0 0 0 4 39 79 48 9 2 1	
187	40 0 0 0 0 1 20 63 62 22 7 1 0	
179	42 0 0 0 0 0 9 43 67 41 19 5 1 0	
186	46 0 0 0 0 0 1 14 49 73 59 29 9 1 0	
199	50 0 0 0 0 0 0 3 22 69 84 67 34 11 0 0	

ORD: 2 6 10 14 18 22 26 30 34 36 38 40 42 46 50

\* RSS taken over all orders, not just sampled orders.

( $\omega=269^\circ$ )

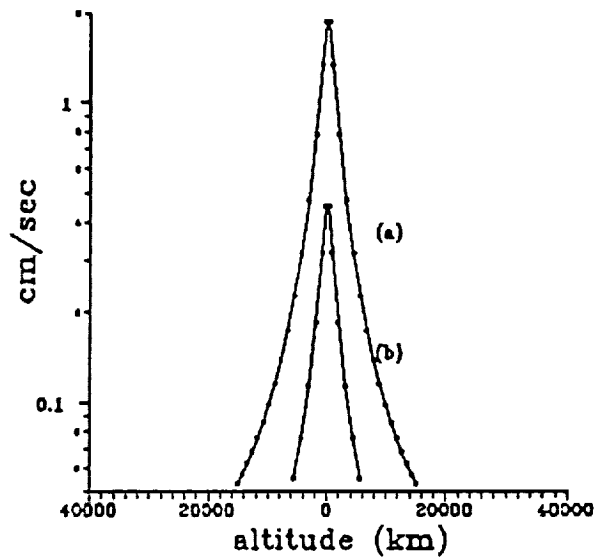
Velocity Perturbations In .001 cm/sec

RSS'	DEG	VKG1: 78-12-20
581650	2 ***	Arg. of periapsis = 269 deg
72711	6 *****	8 day arc length
22705	10 ***494336	
9766	14 *****627 3	
4959	18 *****274 86 1	
2771	22 762***554 37 6 0	
1631	26 148420411 62 11 1 0	
984	30 120 47192 91 2 2 0 0	
604	34 176108 38 65 13 1 1 0 0	
483	36 133175148 45 5 2 0 0 0 0 0	
378	38 157131 40 24 15 1 0 0 0 0 0	
316	40 33 63 81 46 6 2 0 0 0 0 0 0	
244	42 112106 60 6 10 2 0 0 0 0 0 0 0	
162	46 67 69 52 18 2 2 0 0 0 0 0 0 0	
110	50 32 37 35 19 3 1 0 0 0 0 0 0 0 0	

ORD: 2 6 10 14 18 22 26 30 34 36 38 40 42 46 50

\* RSS taken over all orders, not just sampled orders.

Figure 3. Signal Sensitivity by Degree and Order for VO1 Low Orbit



\* based on 8-day arc from epoch 78-01-15

Figure 4. Velocity Perturbation for VO1 Low Orbit due to 25th-Order Harmonic Coefficients for (a): Degrees 31-50, (b) Degrees 41-50\*

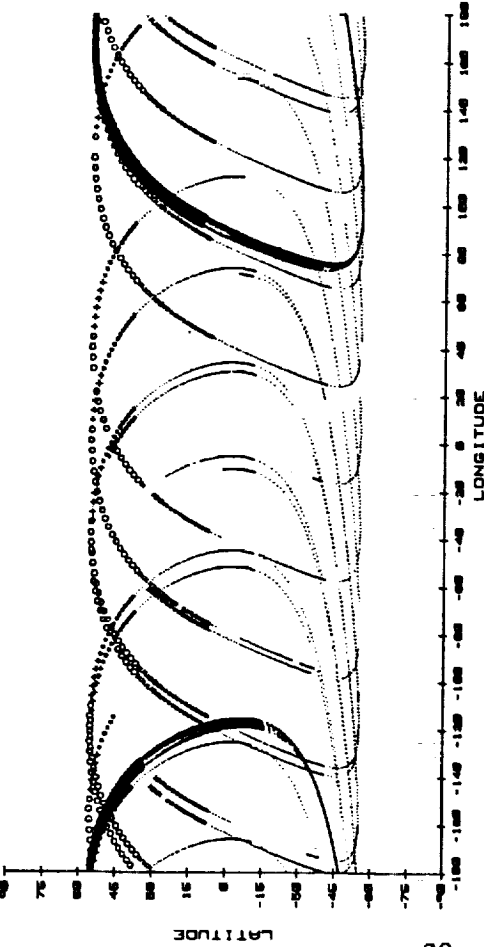
Figure 5a

Data Coverage for Viking-2

Viking-2 1500 km Inc = 55°

- a. Data Span = 16 days Walk = -35°/rev
- b. Data Span = 30 days Walk = -1°/rev

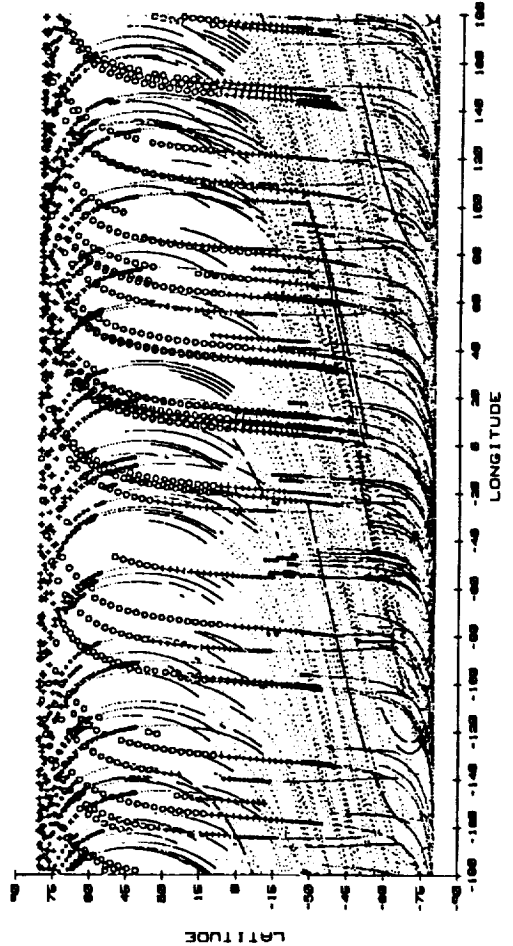
Data Altitude : . >3000 km , \* 3000 to 2000 km , + 2000 to 1700 km , o < 1700 km



Viking-2 800 km Inc = 80°

Data Span = 198 days Walk = mixed ( see Table 2 )

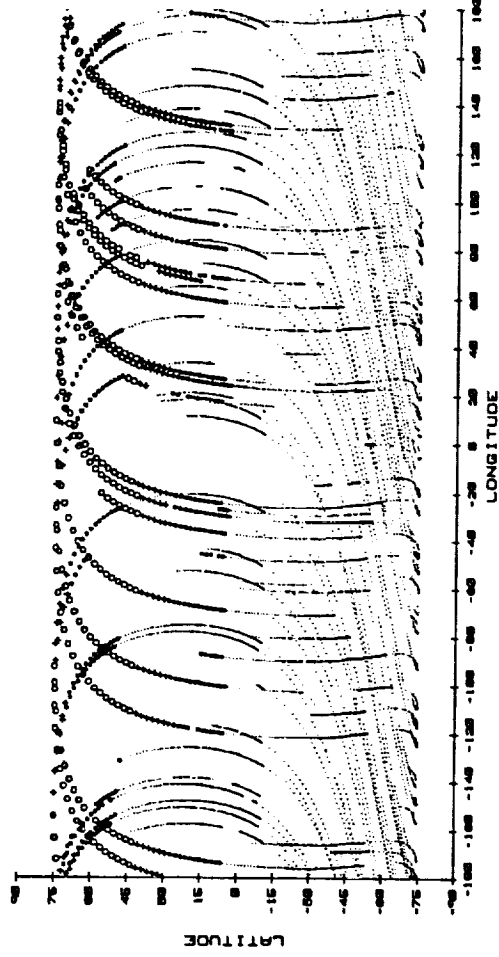
Data Altitude : . >3000 km , \* 3000 to 2000 km , + 2000 to 1000 km , o < 1000 km



Viking-2 1500 km Inc = 75°

Data Span = 35 days Walk = -29°/rev

Data Altitude : . >3000 km , \* 3000 to 2000 km , + 2000 to 1700 km , o < 1700 km



Viking-2 300 km Inc = 80°

Data Span = 155 days Walk = 9°/rev

Data Altitude : . >2000 km , \* 2000 to 1000 km , + 1000 to 500 km , o < 500 km

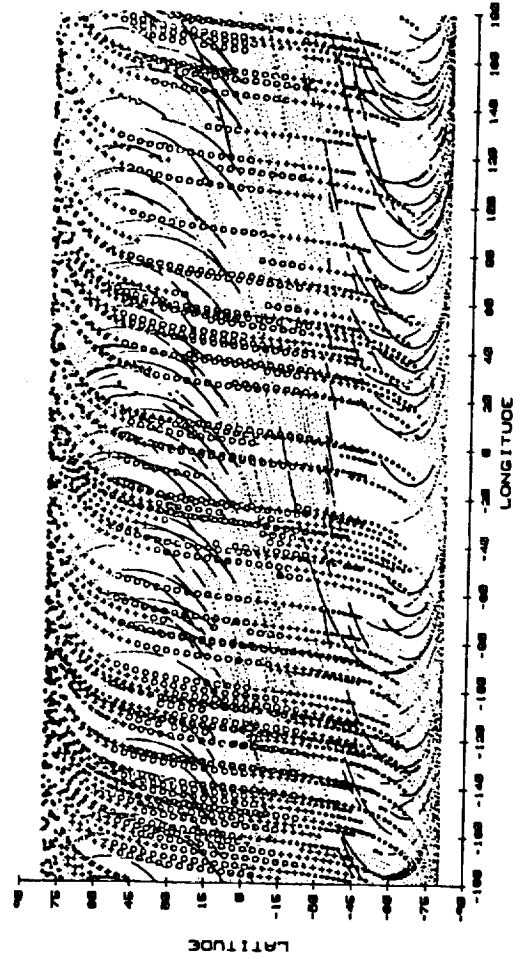


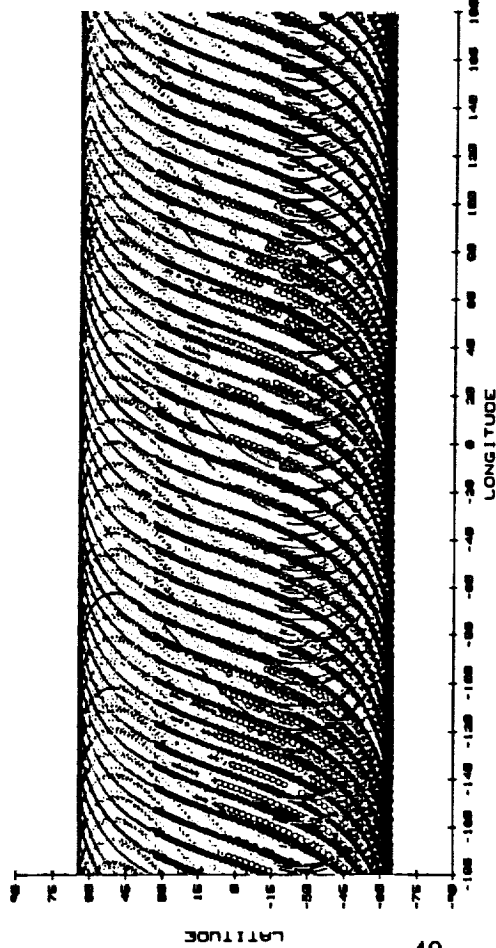
Figure 5b

## Data Coverage for Mariner-9 and Viking-1

**Mariner-9 1500 km Inc = 64°**

Data Span = 138 days Walk = 10°/rev

Data Altitude : : >3000 km , \* 3000 to 2000 km , + 2000 to 1700 km , o < 1700 km



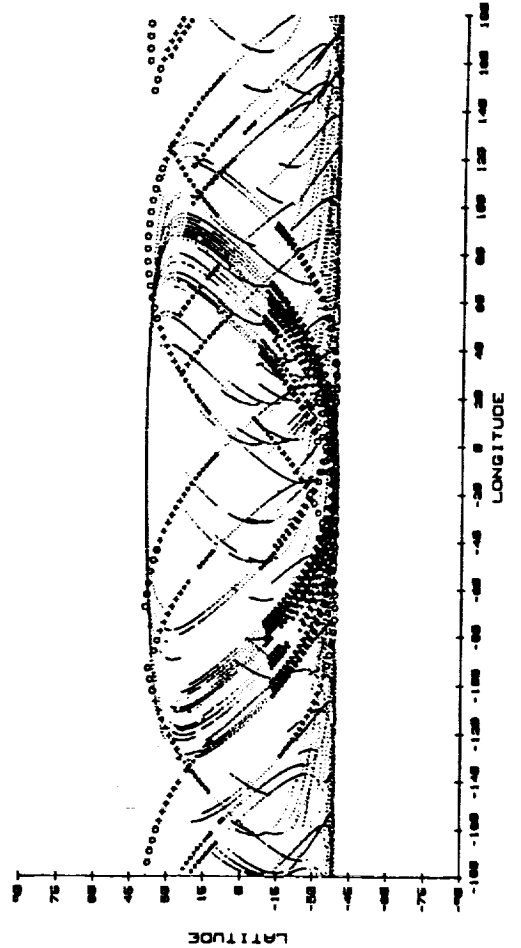
**Viking-1 300 km Inc = 39°**

a. Data Span = 10 days Walk = 43°/rev

b. Data Span = 61 days Walk = 17°/rev

c. Data Span = 16 days Walk = <2°/rev

Data Altitude : : >2000 km , \* 2000 to 1000 km , + 1000 to 500 km , o < 500 km



**Viking-1 1500 km Inc = 39°**

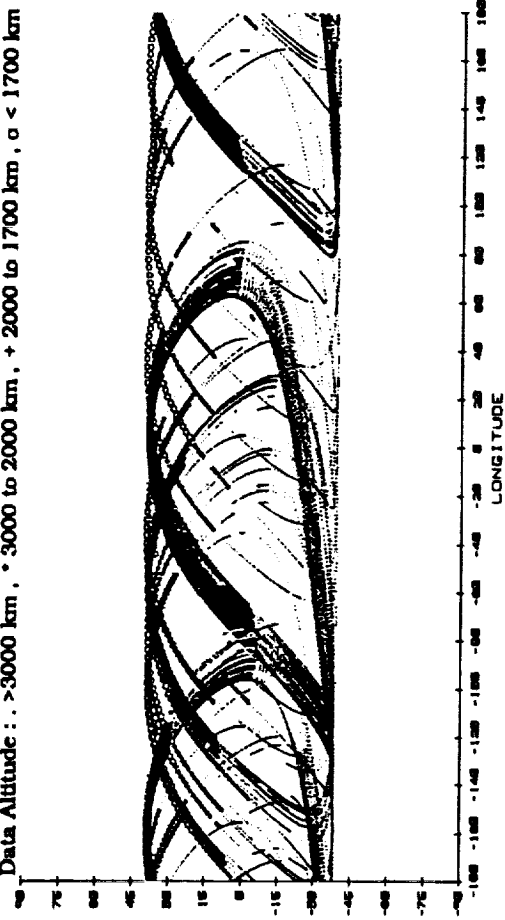
a. Data Span = 44 days Walk = <1°/rev

b. Data Span = 7 days Walk = 44°/rev

c. Data Span = 67 days Walk = <1°/rev

d. Data Span = 18 days Walk = 25°/rev

Data Altitude : : >3000 km , \* 3000 to 2000 km , + 2000 to 1700 km , o < 1700 km



**Viking-1 300 km Inc = 39°**

Data Span = 338 days Walk = 9°/rev

Data Altitude : : >2000 km , \* 2000 to 1000 km , + 1000 to 500 km , o < 500 km

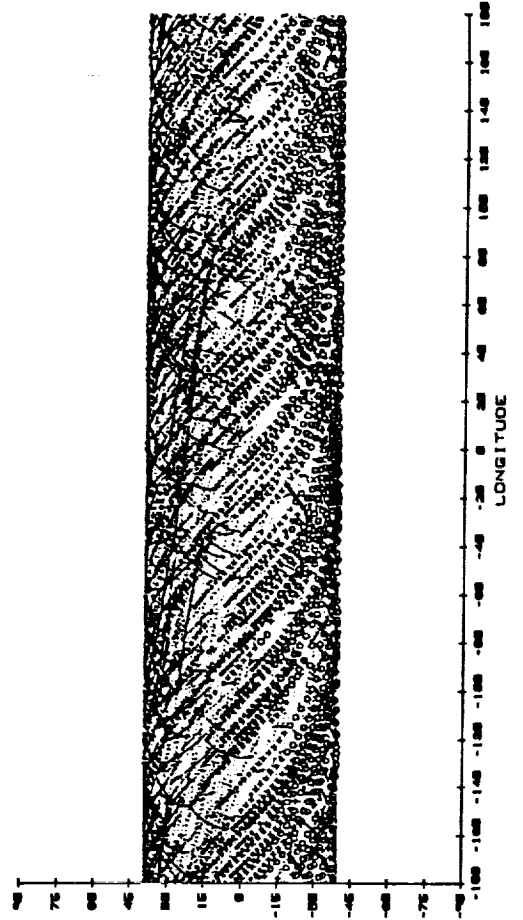
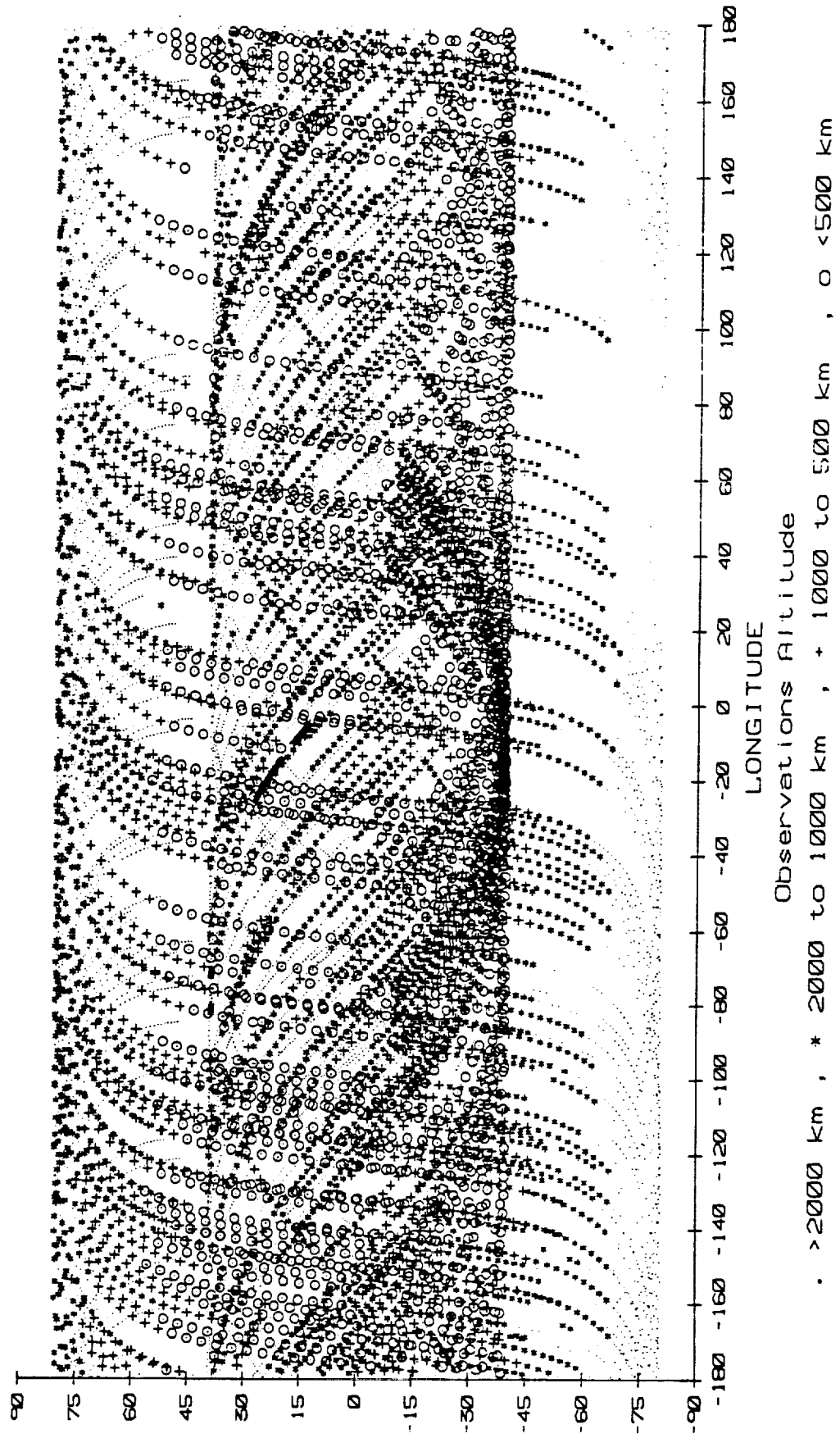


Figure 6

Viking-1 and Viking-2 300 km. Observations with Altitude <5000 km.



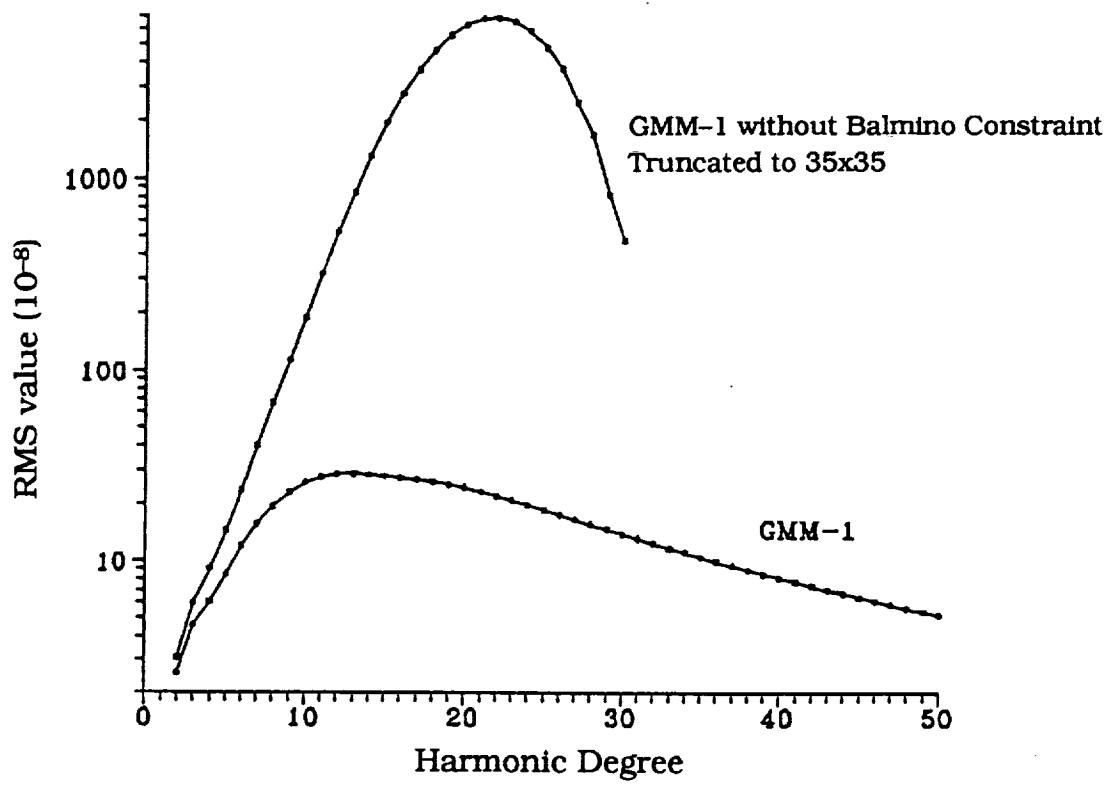


Figure 7. Gravity Model Uncertainties



Figure 8. RMS of Mars Gravity Model Coefficients and Standard Deviations per Degree

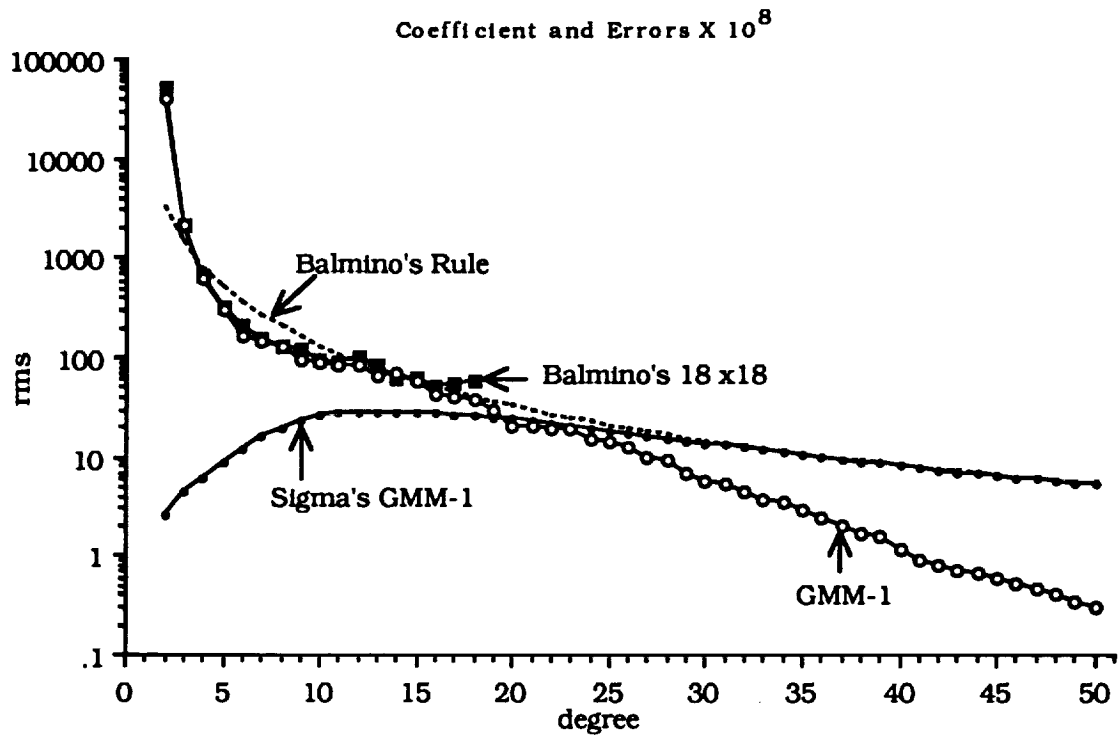


Figure 8. RMS of Mars Gravity Model Coefficients and Standard Deviations per Degree



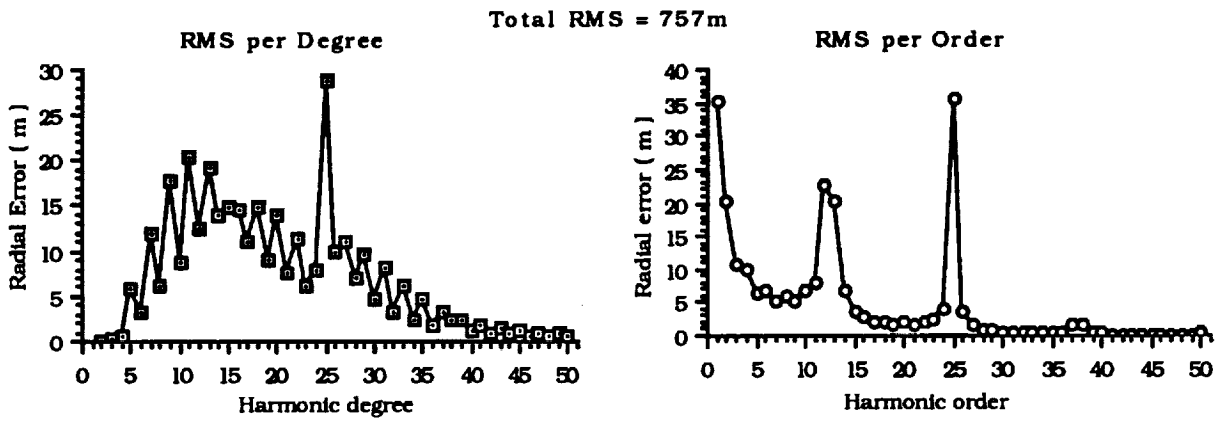


Figure 10. Projected Radial Position Error on Mars Observer from GMM-1 Gravity Covariances

**Figure 11. Projected Along-Track Position Error on Mars Observer from GMM-1 Gravity Covariances**

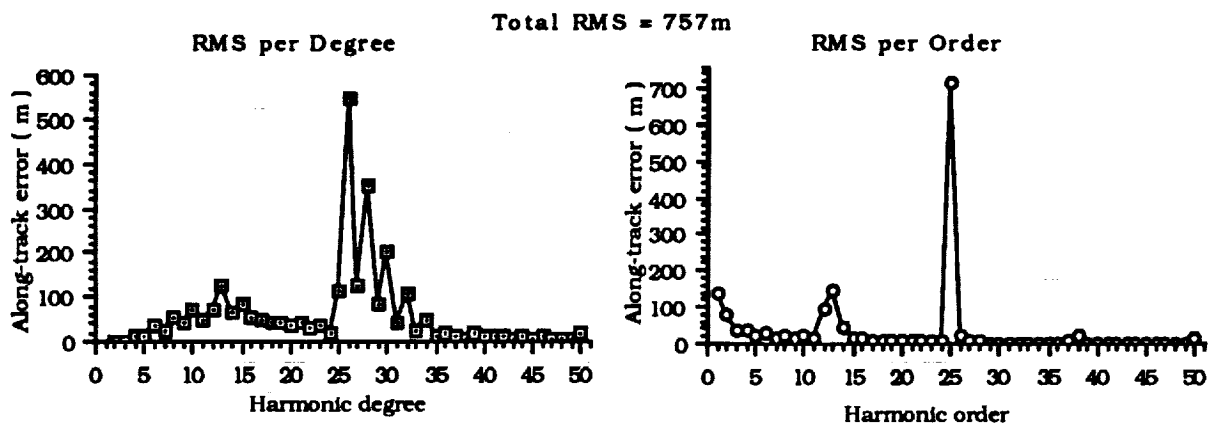
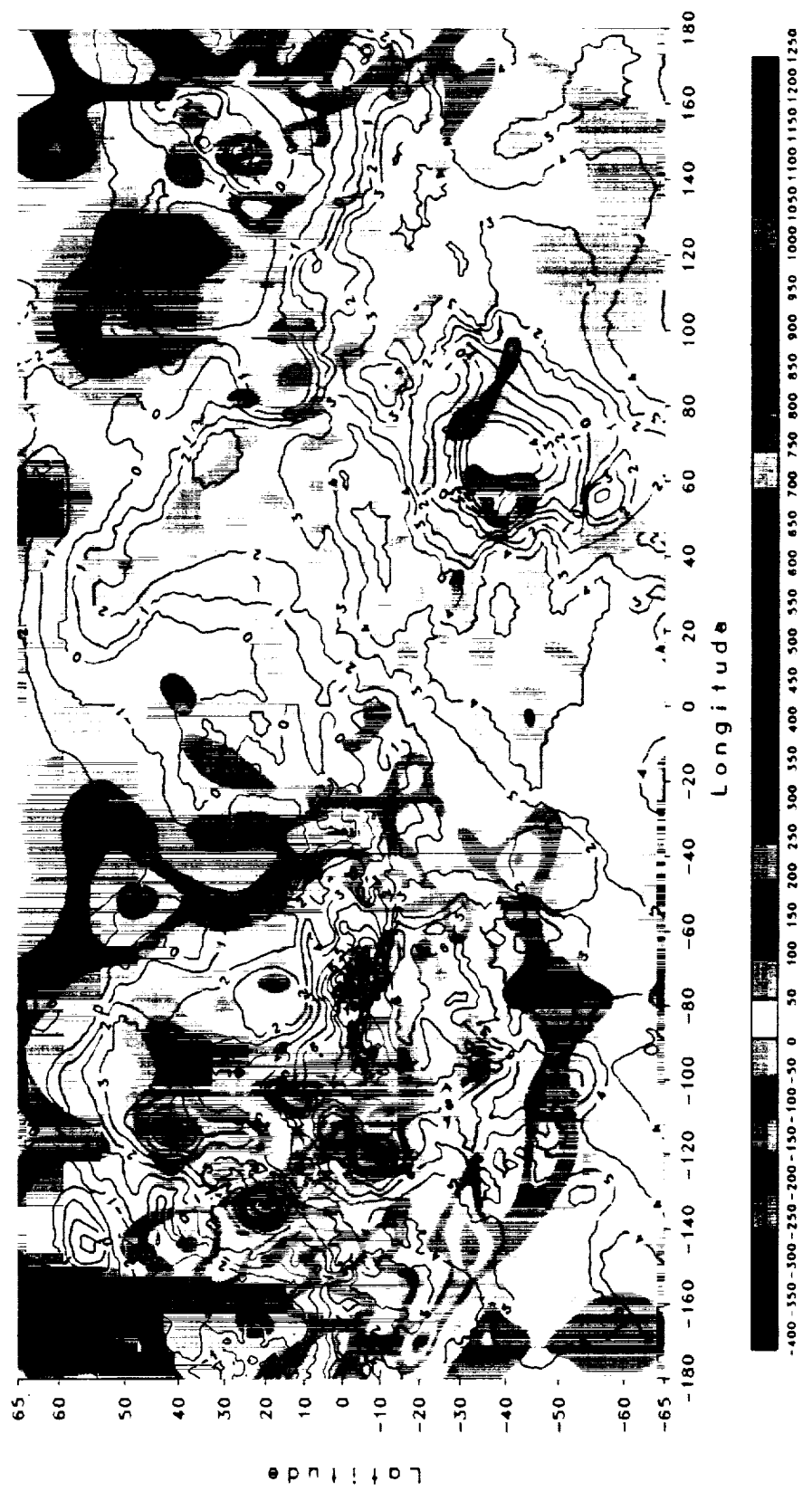


Figure 11. Projected Along-Track Position Error on Mars Observer from GMM-1 Gravity Covariances

Figure 12  
Mars Free Air Gravity Anomalies Computed From GMM-1

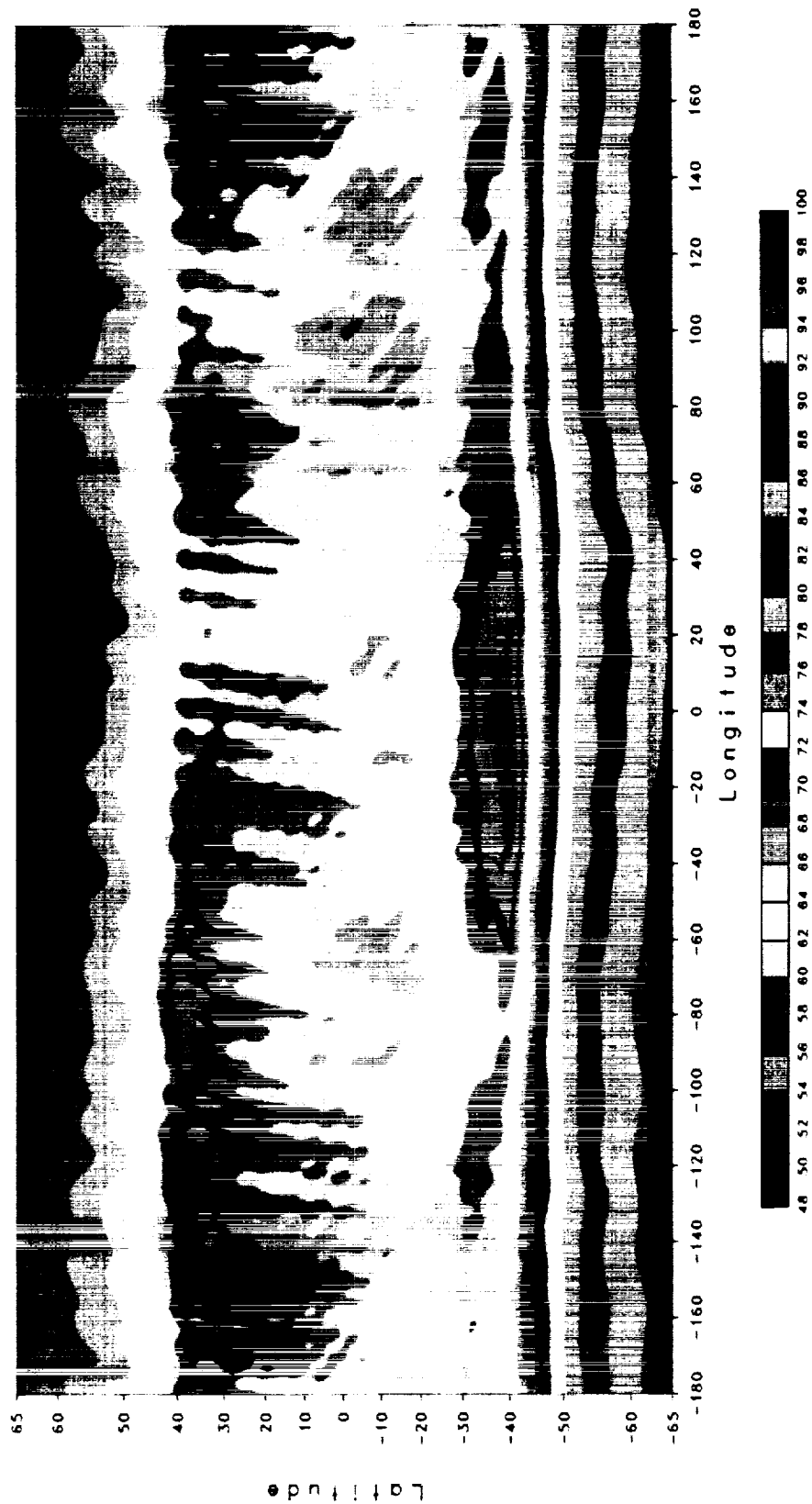
Contour Interval: Anomalies = 50 mgals . Topography = 1 km



[The page contains extremely faint and illegible text, likely a scan of a document with very low contrast or significant noise. The text is mostly centered and appears to be organized into paragraphs or sections, but the individual characters and words are not discernible.]

Figure 13  
Mars Gravity Anomaly Errors from GMM-1

Contour Interval = 2.0 mgals



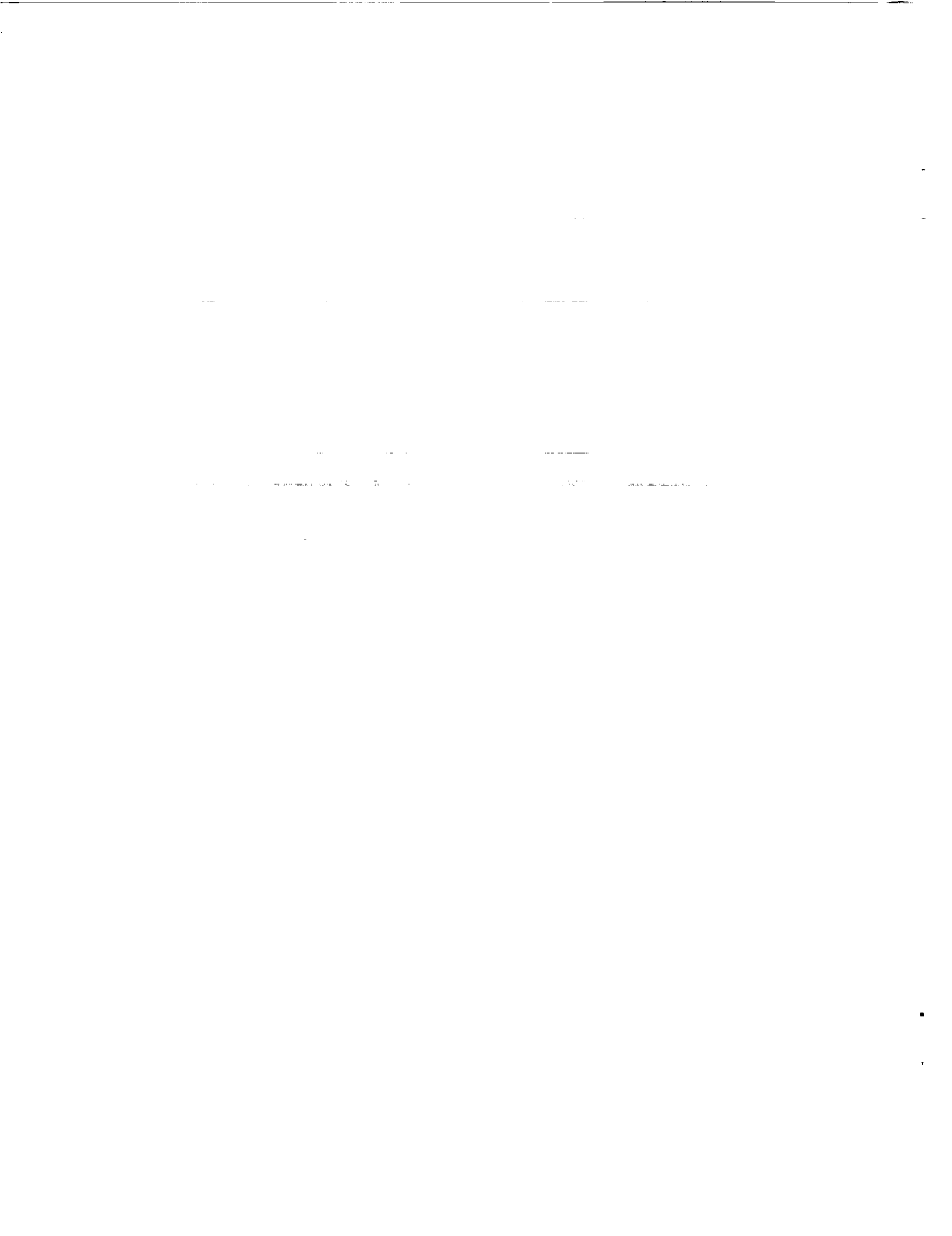
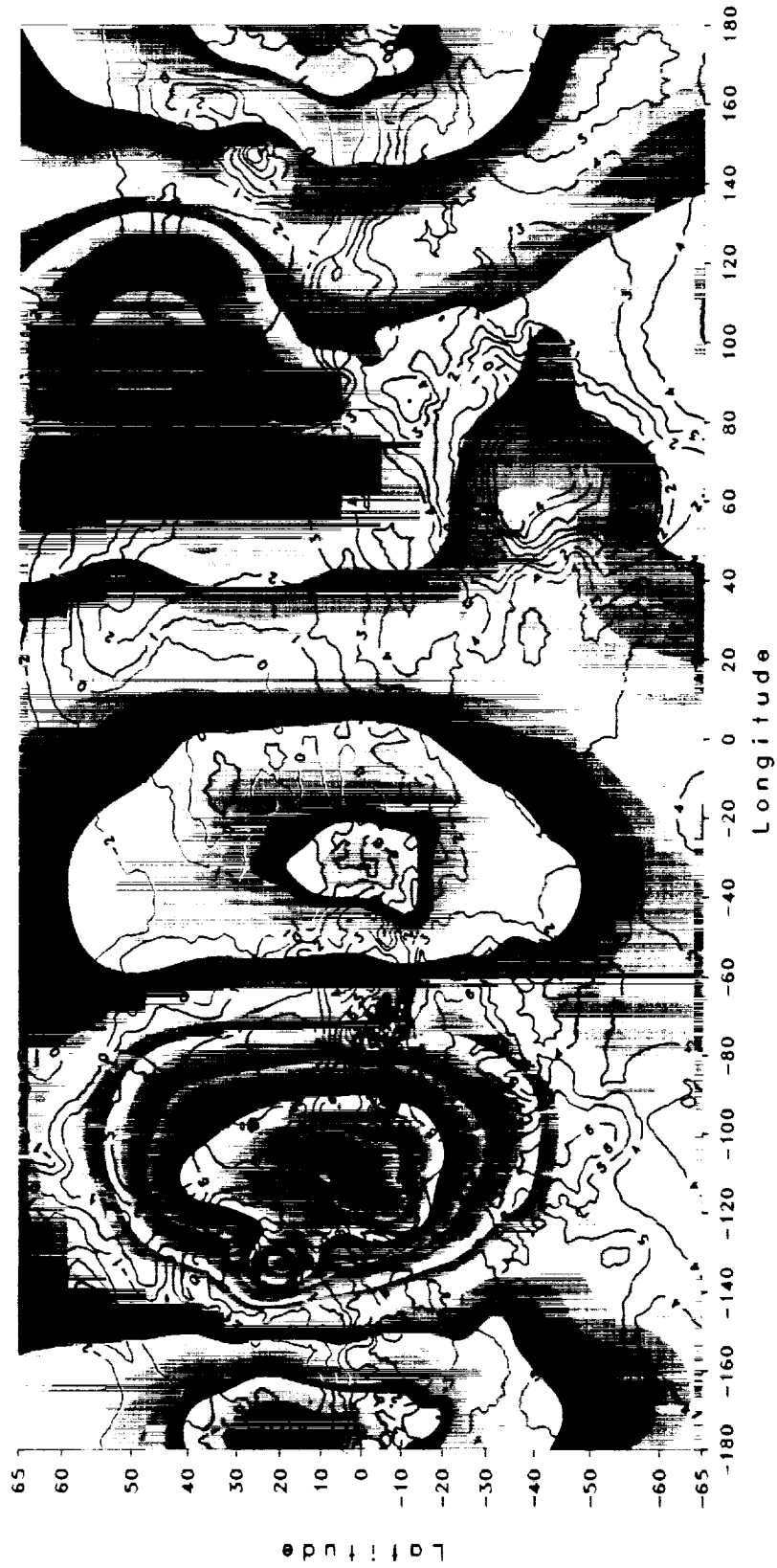




Figure 14  
Mars Geoid Surface Computed From GMM-1

Contour Interval: Heights = 50 m. . Topography = 1 km



-850 -800 -750 -700 -650 -600 -550 -500 -450 -400 -350 -300 -250 -200 -150 -100 -50 0 50 100 150 200 250 300 350 400 450 500 550 600 650 700 750 800 850 900 950 1000 1050 1100 1150 1200 1250 1300 1350 1400 1450



# REPORT DOCUMENTATION PAGE

*Form Approved*  
OMB No. 0704-0188

Public reporting burden for this collection of information is estimated to average 1 hour per response, including the time for reviewing instructions, searching existing data sources, gathering and maintaining the data needed, and completing and reviewing the collection of information. Send comments regarding this burden estimate or any other aspect of this collection of information, including suggestions for reducing this burden, to Washington Headquarters Services, Directorate for Information Operations and Reports, 1215 Jefferson Davis Highway, Suite 1204, Arlington, VA 22202-4302, and to the Office of Management and Budget, Paperwork Reduction Project (0704-0188), Washington, DC 20503.

<b>1. AGENCY USE ONLY (Leave blank)</b>	<b>2. REPORT DATE</b> May 1993	<b>3. REPORT TYPE AND DATES COVERED</b> Technical Memorandum
---	-----------------------------------	---

<b>4. TITLE AND SUBTITLE</b>  An Improved Gravity Model for Mars: Goddard Mars Model-1 (GMM-1)	<b>5. FUNDING NUMBERS</b>  926
--	--------------------------------------

<b>6. AUTHOR(S)</b> D. E. Smith, F. J. Lerch, R. S. Nerem, M. T. Zuber, G. B. Patel, S. K. Fricke, and F. G. Lemoine	
--	--

<b>7. PERFORMING ORGANIZATION NAME(S) AND ADDRESS(ES)</b>  Goddard Space Flight Center Greenbelt, Maryland 20771	<b>8. PERFORMING ORGANIZATION REPORT NUMBER</b>  93B00077
---	---

<b>9. SPONSORING/MONITORING AGENCY NAME(S) AND ADDRESS(ES)</b>  National Aeronautics and Space Administration Washington, D.C. 20546-0001	<b>10. SPONSORING/MONITORING AGENCY REPORT NUMBER</b>  TM-104584
--	--

**11. SUPPLEMENTARY NOTES**  
Zuber: at NASA-GSFC, Greenbelt, MD, and at Department of Earth and Planetary Sciences, Johns Hopkins University, Laurel, MD. Patel: Hughes-STX Corporation, Lanham, MD. Fricke: RMS Technologies, Inc., Landover, MD. Lemoine: University of Colorado, Boulder, CO; NASA-GSFC, and University of Maryland, College Park, MD.

<b>12a. DISTRIBUTION/AVAILABILITY STATEMENT</b> Unclassified-Unlimited Subject Category 46 Report is available from the National Technical Information Service, U.S. Dept. of Commerce, 5285 Port Royal Road, Springfield, VA 22151; (703) 557-4650.	<b>12b. DISTRIBUTION CODE</b>
---	-------------------------------

**13. ABSTRACT (Maximum 200 words)**  
Doppler tracking data of three orbiting spacecraft have been reanalyzed to develop a new gravitational field model for the planet Mars, GMM-1 (Goddard Mars Model-1). This model employs nearly all available data, consisting of approximately 1100 days of S-bank tracking data collected by NASA's Deep Space Network from the Mariner 9, and Viking 1 and Viking 2 spacecraft, in seven different orbits, between 1971 and 1979. GMM-1 is complete to spherical harmonic degree and order 50, which corresponds to a half-wavelength spatial resolution of 200-300 km where the data permit. GMM-1 represents satellite orbits with considerably better accuracy than previous Mars gravity models and shows greater resolution of identifiable geological structures. The notable improvement in GMM-1 over previous models is a consequence of several factors: improved computational capabilities, the use of optimum weighting and least-squares collocation solution techniques which stabilized the behavior of the solution at high degree and order, and the use of longer satellite arcs than employed in previous solutions that were made possible by improved force and measurement models. The inclusion of X-band tracking data from the 379-km altitude, near-polar orbiting Mars Observer spacecraft should provide a significant improvement over GMM-1, particularly at high latitudes where current data poorly resolves the gravitational signature of the planet.

<b>14. SUBJECT TERMS</b>  Gravitational Field, Geodesy, Geophysics, Mars, Deep Space Network (DSN), Doppler Tracking Data, Viking and Mariner Orbits, Orbit Determination and Estimation Theory	<b>15. NUMBER OF PAGES</b> 50
	<b>16. PRICE CODE</b>

<b>17. SECURITY CLASSIFICATION OF REPORT</b> Unclassified	<b>18. SECURITY CLASSIFICATION OF THIS PAGE</b> Unclassified	<b>19. SECURITY CLASSIFICATION OF ABSTRACT</b> Unclassified	<b>20. LIMITATION OF ABSTRACT</b> Unlimited
--	---	--	--

